$f(T)$ Gravity Models and Cosmological Tests

John Soo Yue Han
Department of Physics
National University of Singapore

A thesis submitted for the degree of
B.Sc (Hons) in Physics
2013/14

Abstract

Dark energy may have been widely accepted as the prominent candidate to explain our accelerating universe, but recent studies have shown that $f(T)$ gravity models may be a better solution. These gravity models which stemmed out from the mathematical framework of the teleparallel equivalence of general relativity (TEGR) have been shown to fit several cosmological observational constraints better than the use of a cosmological constant. In this study, I proposed three different two-parameter $f(T)$ functions, and proceed to verify whether they explain the accelerating universe better than the Lambda Cold Dark Matter (ΛCDM) model. This is done by using two-dimensional χ^2 tests to find their best-fit model parameter n and the mass density parameter at present day $\Omega_{m,0}$, using three observational constraints: the Type Ia Supernovae Test (SNE), the combined Cosmic Microwave Background and Baryonic Acoustic Oscillation Test (CMB/BAO) and the Observational Hubble Data (OHD). Various analytical, computational and numerical methods have been used in the study, and the results showed that while a reciprocal power $f(T)$ model fits the observational constraints the best, its results seemed indistinguishable from the ΛCDM model. The value of $\Omega_{m,0}$ obtained from the analysis is consistently found to be around 0.29.

Acknowledgements

First and foremost, I would like to thank my final year project (FYP) supervisor, Dr Cindy Ng for her patience and guidance throughout the past one year. Dr Cindy had been a very kind and helpful lecturer and supervisor: she always gave me room to figure out the physics on my own, and would always help me to find a solution when I got stuck, despite her busy schedule. I would like to express my heartfelt thanks towards her for her great support, both academically and emotionally, and for choosing and shaping a suitable FYP project for me. Also not to forget the random chit-chats we had in her office, her advices regarding matters of the NUS Physics Society when I was the president of the club, her guidance for my UROPS project prior to this, and the numerous recommendation letters she wrote in account for my graduate school and scholarship applications: I sincerely appreciate all her effort throughout the years, and I wish her all the best in her career of lecturing and researching.

Next, I would like to thank all the professors / lecturers that have taught me physics modules throughout the past 4 years, especially thanking them for doing a good job passing down physics knowledge to all the students. I would like to acknowledge a few professors that have made a great impact on my FYP: Dr Wang Qinghai and Dr Kuldip Singh, for their dedication in teaching the modules Relativity and Mathematical Methods in Physics III, in which the solid mathematical foundation they built in me allowed me to understand the tough mathematics in TEGR better; A/Prof Paul Lim, for giving me a good foundation in computational methods in physics, such that I was able to produce good MATLAB codes for this project; And last but not least, A/Prof Phil Chan and Prof Valerio Scarani, for being encouragers and motivators throughout my 4th year in NUS. The random chats with them, the simple words of encouragement they gave have enabled me to persevere in my final year. Sincere thanks to you all.

Here's a short note to thank Mr Lim Teck Seng, one of our physics department's laboratory technologist, who provided me a computer to use in the Honours Student Room. As some of my MATLAB codes run for days and weeks, I couldn't have completed my FYP in time without his help.

Here's a special paragraph to thank all my fellow physics coursemates, who have been supporting me in various ways. Some of them despite their busy schedule have helped me out in my physics modules, and gave me some insights on how to solve some problems in my FYP. Of course, the help does not restrict to only academic ones, it also includes the lunch gatherings at the Science canteen pink tables, *yumcha* and supper times, and most of the time even the simplest "how's your FYP?" greeting helped to

relieve some stress. Here's a special thank-you note to my Physics Christian Fellowship group of friends: Aren, Jacqueline, Theodore, Kim, Kirsten, Meng How, and Yin Chi, thank you all for gathering almost every week to pray for one another in school: you all are my greatest spiritual and emotional support throughout the past 4 years. Also not to forget some of my buddies: Kok Wei, Koon Tong, Mao Tian, Jamil, Melvin, Yingjie, Jing Hao and Nic, thank you all for being there for me. You all played a great role throughout my 4 years of undergraduate physics, I was glad to have you all walk this physics journey together, I couldn't imagine my 4 years without you all.

I would also like to thank the Ministry of Foreign Affairs of Singapore and 1Malaysia Development Berhad for supporting me financially throughout my undergraduate course in NUS. Last but not least, I also want to express my heartfelt thanks to my adoptive parents for believing in me, encouraging me, and supporting me as I walk through this undergraduate journey. I love you both. I also want to tell my mother in heaven, "Mommy, I've fulfilled your will, I have completed my undergraduate degree!"

I give praise to God for placing all these people in my life and for making me get to where I am today. *All glory to God!*

John Soo Yue Han
NUS, Singapore
March 31, 2013

List of Figures

List of Tables

Contents

Chapter 1

INTRODUCTION

1.1 The Universe As We See It

The universe that we live in had always been a mystery to mankind. How it began, what is happening to it now, and what will it become in the future: these are just a few of the questions that scientists have been working hard to sought for a reliable answer. These are important questions, as a further understanding about this mysterious black void space is essential for the survival of the human race in the distant future. A better understanding on our universe might be able to save us from catastrophes that we do not foresee.

To understand the universe, we first have to observe it. After observing it, we then need to come up with physical theories to explain why it behaves as it is. Since the renaissance era of science and technology, physicists have made huge progress into understanding it better. Just 100 years ago, we had Albert Einstein coming up with general relativity to explain the universe as a geometrical structure; 50 years later, we have set our feet on the moon. Not longer than 20 years ago, we found out that the universe not only has been expanding, but expanding at an accelerating rate. And in the recent years, many scientists and research groups has been working hard to explain this acceleration using various kinds of theories, and fitting these theories with various kinds of observational constraints.

While general relativity is well known by most students who study physics, it has a lesser known counterpart known as teleparallel gravity, which also serves the same purpose to explain the shape and structure of the universe in mathematical equations. General relativity and teleparallel gravity are fundamentally and theoretically different from one another: in simple words, general relativity uses curvature to describe gravity, while teleparallel gravity uses torsion instead. Teleparallel gravity is not new: it had been around since the 1920s, and currently many physicists have revived this theory to work on new alternatives to the cosmological constant. One prominent method is to modify teleparallel gravity into $f(T)$ gravity (also known as torsion gravity), in which the whole bulk of this thesis will be about.

1.2 Motivation

In the recent years, there are many online literatures which use $f(T)$ gravity to explain the accelerating universe. In the recent 2010, Wu et al had studied the observational constraints on $f(T)$ gravity.[1] From then on, $f(T)$ gravity models had been studied by various groups of people in various aspects: Keisuke and team studied the perturbations of $f(T)$ gravity,[2] Wu and team proceeded to study its phantom divide line crossing,[3] but most research groups introduced new distinct $f(T)$ functions to fit our current observational constraints.

This project is motivated by the ongoing researches on $f(T)$ models, and the intention to study how $f(T)$ functions are formulated, what are the other possible forms of $f(T)$ functions, which $f(T)$ function fits our observational tests the best, and ultimately to determine whether $f(T)$ gravity is a promising alternative to dark energy. Thus in this project, the teleparallel equivalence of general relativity will be studied, a few new $f(T)$ functions will be formulated, and χ^2 tests will be used against observational data to test the validity of these functions. After comparing them with one another, a conclusion will be drawn.

1.3 Outline of this Thesis

This thesis will begin with a theoretical overview of general relativity, and will include the equations and concepts needed to understand the structure of the universe. Then the teleparallel gravity theory will be introduced, it will be compared with general relativity so that the reader will know their similarities and its advantages over general relativity. After that, the discussion will turn to how general relativity and teleparallel gravity have to be modified in order to account for the accelerating universe, and thus the introduction of dark energy (the cosmological constant), modified-gravity / modified-matter theories, and finally the introduction of $f(T)$ gravity.

After laying down the foundations of the theory, this thesis will proceed to discuss how these theories / models can be verified, which is through observational constraints. 5 different observational constraints will be discussed, and information on the sources of these tests, the data measured and the reliability of the tests will be presented. These 5 observational constraints are the type Ia supernovae test (SNE), cosmic microwave background (CMB), baryonic acoustic oscillation (BAO), observed Hubble data (OHD) and gamma ray bursts (GRB).

At this point, the reader should have sufficient knowledge on the background and theory of $f(T)$ gravity, thus the methodologies will be introduced: the thesis

proceeds to explain the computational, statistical and numerical methods used to obtain the results of this work. These methods include introduction to the χ^2 tests, numerical root finding methods and integration methods. This thesis will then end with the tabulation of results, the discussion of results, the conclusion and the suggestions for future work.

Chapter 2

THEORETICAL OVERVIEW OF $f(T)$ GRAVITY

2.1 Introduction

This section will be a step-by-step process to help the readers understand the basics of $f(T)$ gravity. Instead of jumping straight into explaining what $f(T)$ gravity is, this section will start with an overview of general relativity, which is what most readers are more familiar with. Teleparallel gravity will be introduced after the foundations of general relativity have been laid: its history, its underlying principles and the motivation to study it will be discussed. It will later be compared with general relativity so that the reader will identify the differences and similarities between the two theories. After that, the reader will be introduced to the accelerating universe and the need to modify these theories to explain this phenomenon. This is where $f(T)$ gravity comes into the picture: it is one of the many methods used to explain the cosmic acceleration through the approach of teleparallel gravity. There are also many approaches from general relativity to explain the cosmic acceleration too, but only the cosmological constant and $f(R)$ gravity will be discussed in this work, and the reader can compare their similarities with $f(T)$ gravity.

2.2 General Relativity

The Metric

In general relativity, it is said that space and time are treated with equal footing. Gravity is introduced as a geometrical structure, and our equations work in a 4-dimensional spacetime, with coordinates (t, x, y, z). General relativity suggests that the gravitational field and force that we know is generated from the geometry of spacetime itself, and all the information on how gravity will act on the mass particles held in that particular space will be contained in the *metric tensor*. For example, a flat spacetime follows the metric of the *Minkowski space*:

$$ds^2 = c^2dt^2 - dx^2 - dy^2 - dz^2. \qquad (1)$$

As it can be seen, a metric is something like a coordinate system, and in this case, it is just a Cartesian coordinate, with an extra time coordinate having a different sign

from the rest. The universe that we know however, might not be flat as Minkowski suggested, and it might not even be static. Most scientists would agree that the best metric to describe our current universe is the Friedman-Lemaître-Robertson-Walker (FLRW) metric,

$$ds^2 = c^2dt^2 - a^2(t)\left[\frac{dr^2}{1-kr^2} + r^2d\theta^2 + r^2\sin^2\theta\, d\phi^2\right] \qquad (2)$$

where $k = -1,0,1$ characterizes the flatness of the universe, being closed, flat and open universe respectively. A closed universe has its geometry like the surface of a sphere, it will expand, and eventually contract back again to a singularity, also known as the 'Big Crunch'. The open and flat universe on the other hand, would expand forever, and might end up with a 'Big Freeze' or a 'Big Rip' at different rates.[4] $a(t)$ is the scale factor, it is assumed to be a time dependent radius of the universe. Thus if we have a universe expanding at constant velocity, it will have a positive first derivative, and so on. The FLRW metric defines the geometry of our current universe, and current observations have shown that $k = 0$ seems to be the best fit.[5]

Curvature

The open-ness, close-ness and flat-ness of the universe are concepts of *curvature*. A closed universe has positive curvature, an open universe has negative curvature, and a flat universe has zero curvature. The curvature has significant effects on how vectors are transported from one point to another, affecting where it should be pointing based on how the space is curved. Consider a vector $A^i(\lambda)$. In Euclidean geometry, we know that when the vector moves from x^μ to $x^\mu + \delta x^\mu$, we get the small change in A^i to be $A^i(x^\mu + \delta x^\mu) = A^i(x^\mu) + \frac{\partial A^i(x^\mu)}{\partial x^\mu}\delta x^\mu$. However in a curved space (non-Euclidean geometry), we need to include the concept of *parallel transport*, which is to maintain the direction of the vector when we move along a 'straight' line according to that space.[5] The changes to the components of A^i through parallel transport will be proportional not only to the displacement δx^μ, but also the original component A^i itself. Thus the vector moving from x^μ to $x^\mu + \delta x^\mu$ would have a derivative known as the *covariant derivative*,

$$\nabla_k A^i = \frac{\partial A^i}{\partial x^k} + \Gamma^i_{lk}A^l. \qquad (3)$$

The mathematical rule here, is that this covariant derivative must always transform as a tensor. Γ^i_{kl} is known as the *Christoffel symbol*, collectively they are components of the *Levi-Civita Connection*. Γ^i_{kl} can be derived from the equation of motion, and is related to the metric through the equation

$$\Gamma_{kl}^{i} = \frac{1}{2} g^{ij} \left(\partial_k g_{jl} + \partial_l g_{jk} - \partial_j g_{kl} \right) \tag{4}$$

where $\partial_k = \frac{\partial}{\partial x^k}$, and g_{ij} is the FLRW metric, which is just equation (2), or more precisely, $g_{00} = 1, g_{11} = -\frac{a^2(t)}{1-kr^2}, g_{22} = -a^2(t)r^2$ and $g_{33} = -a^2(t)r^2 \sin^2\theta$. The index 0 refers to the time component, and the indices 1, 2 and 3 refer to the space component. In general relativity, this Levi-Civita connection is formulated with the conditions that spacetime is torsionless $\left(\Gamma_{kl}^{i} = \Gamma_{lk}^{i}\right)$ and that the metric is preserved $\left(\nabla_i g_{jk} = 0\right)$. Therefore, a spacetime metric with non-zero Christoffel symbols equates a curved spacetime.

Having said that, whether a space is curved is more rigorously defined by studying the possibility to transport a vector (say, A^i) between two points without the result dependent on the path. If the vector transports independent of the path, the spacetime is flat, and from equation (3) we will arrive at

$$\frac{\partial A_i}{\partial x^k} - \Gamma_{ik}^{l} A_l = 0. \tag{5}$$

Doing a second derivative to the equation, and using the fact that the order of indices of second derivatives can be switched, we will arrive at the necessary condition for flatness,

$$\frac{\partial \Gamma_{ik}^{m}}{\partial x^n} - \frac{\partial \Gamma_{in}^{m}}{\partial x^k} + \Gamma_{ln}^{m}\Gamma_{ik}^{l} - \Gamma_{lk}^{m}\Gamma_{in}^{l} = R^{m}{}_{ikn} = 0 \tag{6}$$

where $R^{m}{}_{ikn}$ is the *Riemann Curvature Tensor*. As it suggests, the spacetime is flat if the Riemann Tensor vanishes everywhere. Taking the trace of $R^{m}{}_{ikn}$, we then get the *Ricci Tensor*,

$$R_{\alpha\beta} = R^{\epsilon}{}_{\alpha\epsilon\beta} = \partial_\epsilon \Gamma_{\alpha\beta}^{\epsilon} - \partial_\beta \Gamma_{\alpha\epsilon}^{\epsilon} + \Gamma_{\alpha\beta}^{\epsilon}\Gamma_{\epsilon\rho}^{\rho} - \Gamma_{\alpha\rho}^{\epsilon}\Gamma_{\beta\epsilon}^{\rho}. \tag{7}$$

Technically, the Ricci Tensor controls the growth rate of the volume of the metric in the spacetime. Thus the difference in geometry between an ordinary Euclidean n-space and the Riemannian spacetime can be determined by the information provided in the Ricci Tensor.[6] The tensor can be further contracted to give the *Ricci scalar*,

$$R = g^{ik} R_{ik}. \tag{8}$$

The Ricci scalar also acts as a mathematical object to compare the deviation of volume between a Euclidean space and spacetime, but in this case it is metric dependent, while the previous two tensors could be defined from any affine connection.[7]

Einstein-Hilbert Action & Einstein Field Equation

The Ricci scalar plays an important role in general relativity, as it happens to be the Lagrangian density of *Einstein-Hilbert action*,

$$S = \int \left(\frac{c^4}{16\pi G} R + \mathcal{L}_M \right) \sqrt{-g}\, d^4x. \tag{9}$$

Here $\mathcal{L}_M$ is the Lagrangian density describing any matter fields in the spacetime, while g is the determinant of the metric. An action is an attribute of the dynamics of a physical system, it is a mathematical functional which takes the trajectory of the system as its argument, and it outputs a real number.[8] Using the principle of least action ($\delta S = 0$) and a lot of mathematics, we arrive at the famous *Einstein's field equation*,

$$R_{\mu\nu} - \frac{1}{2} g_{\mu\nu} R = \frac{8\pi G}{c^4} T_{\mu\nu}. \tag{10}$$

$T_{\mu\nu}$ is the *energy-momentum tensor*, which contains the information of all the constituents (radiation, baryonic and non-baryonic matter) in our universe, is the part derived from $\mathcal{L}_M$. More precisely, T_{00} is the energy density, $T_{i0} = T_{0i}$ is the momentum density (or energy flux) and T_{ij} is the stress tensor.[9] Einstein's equation is an equation of motion, the equation tells us that the existence of energy and matter would bend the spacetime around it, causing the Newtonian 'gravitational force' as we know when two massive bodies are close to one another.

One last equation in this section to be introduced would be the *geodesic equation*,

$$\frac{d^2 x^\mu}{d\tau^2} = -\Gamma^\mu_{\alpha\beta} \frac{dx^\alpha}{d\tau} \frac{dx^\beta}{d\tau}. \tag{11}$$

This equation is derived by extremizing the proper time τ along a timelike world line using the Euler-Lagrange equation. The geodesic equation generally tells us that free falling motion may be curved, and depending on the curvature of the spacetime, the shortest distance between two points may not be a 'straight' line. So this geodesic equation together with Einstein's equation will dictate how free-falling objects move in spacetime, and these are the fundamental mathematics of general relativity.

In summary, once we know the metric and the constituents of a spacetime, we can derive information on its curvature, and further deduce how matter and radiation react in such a spacetime through an equation of motion. General relativity, in simple words, says that the geometry of spacetime affects how the particles in it interact with one another.

2.3 Teleparallel Gravity

Teleparallel gravity is also known as the teleparallel equivalence of general relativity, or teleparallelism in the older days. As mentioned earlier, this theory serves to explain gravitation using equations, just like general relativity. However, this theory is very different and much more complicated than general relativity, among the most important aspects are that teleparallel gravity imposes zero curvature, while general relativity assumes zero torsion. Teleparallel gravity is much more mathematically involved, it requires advanced knowledge in differential geometry for readers to understand it better. For the interest of the reader, the following section will be a brief history of the formulation of this theory, and the explanation of the theory will come in the next subsection.

2.3.1 History

When general relativity was formulated in the 1900s, efforts had been made to unify gravity with electromagnetism. The first person who started the effort was none other than H. Weyl, whom although didn't succeed, had laid the foundations of what we know today as gauge theory and invariances.[10] In the 1920s, Albert Einstein worked on the mathematical structure of teleparallelism, he introduced a tetrad (a field of orthonomal bases) on a tangent space, which had 16 independent components to unify gravity and electromagnetism. Unlike the spacetime metric which had only 10 independent components, he wanted to use the extra 6 components to include electromagnetism. However, his efforts failed.

While teleparallelism included the concept of torsion without curvature, Cartan formulated an even more general idea of spacetime around the same time. This was the birth of the *Einstein-Cartan Theory*, in which he suggests that torsion and curvature are separate degrees of freedom, and predicted that while energy and momentum are the source of curvature, something has to be the source of torsion (much later proven to be spin).[10]

Teleparallelism was left alone for quite some time, until 1961 when Møller used it for a different purpose, which was to find a tensorial complex for the gravitational

energy-momentum density, in which however wasn't invariant under local Lorentz transformation. Following his work, Hayashi and Nakano formulated the gauge theory for teleparallelism in the translation group.[10] Then in 1962, Plebanski and Pellegrini formulated the Lagrangian for teleparallel gravity, and it was then proven by Cho to be equivalent to the Einstein-Hilbert Lagrangian up to a divergence term under local Lorentz transformation.[10]

From the 1970s onwards, many physicists had been fine-tuning the fundamentals of teleparallelism, properly constructing and defining the many terms involved, which in turn became what we know today as the *teleparallel equivalence of general relativity*, or teleparallel gravity. Many research groups in the recent years had been working on teleparallel gravity, modifying it into torsion gravity as an alternative to the cosmological constant to explain the our accelerating universe.

2.3.2 Theory

Teleparallel gravity can be interpreted as a gauge theory for the translation group. Unlike general relativity, it has no geodesics, but instead uses torsion as a source of 'force' just like the Lorentz force in electromagnetism.[11] Because of that, teleparallel gravity does not need the equivalence principle to be valid. This is important since the equivalence principle in which general relativity is constructed on has faced some problems at the quantum level. As the theory of teleparallel gravity is highly technical, the following paragraphs will only act as a simple introduction to teleparallel gravity, it should provide the bare minimum knowledge enough for the reader to understand what this project is about. The tedious calculations and derivations will be omitted.

Some Basic Differential Geometry

General relativity works in the Riemannian spacetime, where torsion T vanishes everywhere. Teleparallel gravity on the other hand, works in the *Weitzenböck spacetime*, in which the curvature R vanishes instead. These two spacetimes belong under the umbrella of the generalized Riemann-Cartan spacetime, in which the curvature and torsion are non-zero. Incidentally, we are also familiar of the Minkowski spacetime, in which both curvature and torsion are zero. These concepts are visually summarized in **Fig. 1** in the next page. From the figure, it can be seen that teleparallel gravity is just another way of explaining gravity, and it acts as the complement to general relativity.

In order to further explain the concepts of teleparallel gravity, we need to move away from our comfortable spacetime coordinates into a more generalized mathematical space, which is the manifold of tangent space. From this point onwards,

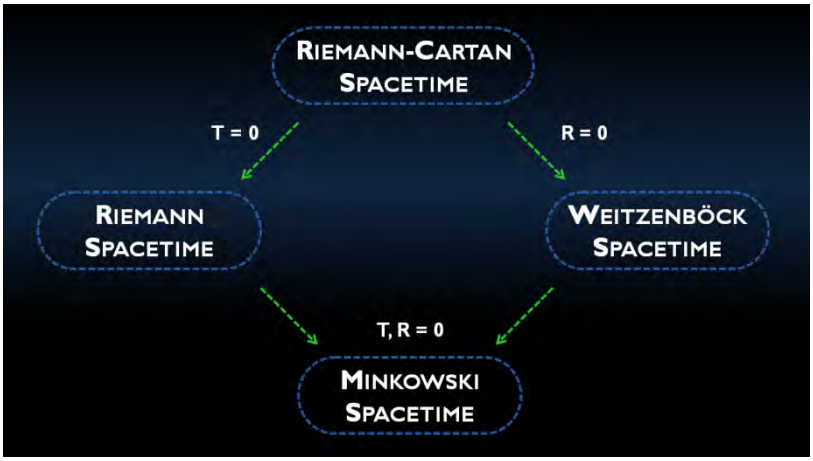

Fig. 1: Concept Map of The Different Spacetimes[12]

Greek alphabets will be used to denote indices of spacetime, while Latin alphabets will be used to denote indices in the tangent space. Firstly, we need the setup of a non-trivial tetrad $h^a{}_\mu$, a set of 4 orthonomal vector fields physically used to interpret spacetime. The tetrad is related to the metric by the following equation:

$$g_{\mu\nu} = \eta_{ab} h^a{}_\mu h^b{}_\nu. \tag{12}$$

In this general tangent space, we need to redefine our connection $\check{\Gamma}^\gamma{}_{\alpha\beta}$ to include components which general relativity neglected. A connection is a general term which defines the idea of transporting data along a family of curves. In other words, the affine connection tells us how vectors are differentiable in their nearby points, it allows the connection of nearby tangent vector fields.[13] The expression of the general connection is as follows:

$$\check{\Gamma}^\rho{}_{\nu\mu} = h_a{}^\rho \partial_\mu h^a{}_\nu + h_a{}^\rho A^a{}_{b\mu} h^b{}_\nu \tag{13}$$

where $A^a{}_{b\mu}$ is called the *spin connection*, a connection on the spinor bundle. This equation could also be re-written as

$$A^a{}_{b\mu} = h^a{}_\nu \partial_\mu h_b{}^\nu + h^a{}_\nu \check{\Gamma}^\nu_{\rho\mu} h_b{}^\rho. \tag{14}$$

Just like the Levi-Civita connection $\Gamma^\rho{}_{\nu\mu}$, the affine connection defines the covariant derivative, and it should be the more general form. The general covariant derivative now becomes

$$\mathrm{D}_k A^i = \partial_k A^i + \check{\Gamma}^i_{lk} A^l. \tag{15}$$

This equation will be revisited later.

Curvature and Torsion Tensor

Now that we understand how connection works, we proceed to define our general curvature and torsion tensors,

$$\check{R}^{a}{}_{b\nu\mu} = \partial_\nu A^{a}{}_{b\mu} - \partial_\mu A^{a}{}_{b\nu} + A^{a}{}_{e\nu}A^{e}{}_{b\mu} - A^{a}{}_{e\mu}A^{e}{}_{b\nu} \tag{16}$$

$$\check{T}^{a}{}_{\nu\mu} = \partial_\nu h^{a}{}_{\mu} - \partial_\mu h^{a}{}_{\nu} + A^{a}{}_{e\nu}h^{e}{}_{\mu} - A^{a}{}_{e\mu}h^{e}{}_{\nu}. \tag{17}$$

These are how the curvature and torsion tensors look like in differential geometry, and later we will see that the equations in general relativity are just the special case of this general notation. Using equation (14), indeed we can re-write these two equations in purely spacetime form,

$$\check{R}^{\rho}{}_{\lambda\nu\mu} = h_a{}^{\rho}h^{b}{}_{\lambda}\check{R}^{a}{}_{b\nu\mu} = \partial_\nu \check{\Gamma}^{\rho}{}_{\lambda\mu} - \partial_\mu \check{\Gamma}^{\rho}{}_{\lambda\nu} + \check{\Gamma}^{\rho}{}_{\eta\nu}\check{\Gamma}^{\eta}{}_{\lambda\mu} - \check{\Gamma}^{\rho}{}_{\eta\mu}\check{\Gamma}^{\eta}{}_{\lambda\nu} \tag{18}$$

$$\check{T}^{\rho}{}_{\nu\mu} = h^{\rho}{}_{a}\check{T}^{a}{}_{\nu\mu} = \check{\Gamma}^{\rho}{}_{\mu\nu} - \check{\Gamma}^{\rho}{}_{\nu\mu} \tag{19}$$

Here it has to be noted that $\check{\Gamma}^{\rho}{}_{\mu\nu} \neq \Gamma^{\rho}{}_{\mu\nu}$, as the terms without the 'checks' are reserved for the usual notations in general relativity. To further understand how these two equations turn out differently in the Riemann and Weitzenböck spacetime, we can rewrite equation (13) as[11]

$$\check{\Gamma}^{\rho}{}_{\mu\nu} = \underbrace{\frac{1}{2}g^{\rho\sigma}\left(\partial_\mu g_{\nu\sigma} + \partial_\nu g_{\mu\sigma} - \partial_\sigma g_{\mu\nu}\right)}_{\text{Levi-Civita Connection, } \Gamma^{\rho}{}_{\mu\nu}} + \underbrace{\frac{1}{2}\left(\check{T}_{\nu}{}^{\rho}{}_{\mu} + \check{T}_{\mu}{}^{\rho}{}_{\nu} - \check{T}^{\rho}{}_{\mu\nu}\right)}_{\text{Contorsion Tensor, } \check{K}^{\rho}{}_{\mu\nu}}. \tag{20}$$

The equation $\check{\Gamma}^{\rho}{}_{\mu\nu} = \Gamma^{\rho}{}_{\mu\nu} + \check{K}^{\rho}{}_{\mu\nu}$ helps us to identify how it reverts back to its better-known form in general relativity. By definition, the Riemann spacetime is torsionless $\left(\check{\Gamma}^{\rho}{}_{\mu\nu} = \check{\Gamma}^{\rho}{}_{\nu\mu}\right)$, so equation (19) immediately gives us $\check{T}^{\rho}{}_{\nu\mu} = T^{\rho}{}_{\nu\mu} = 0$. With this information, we see that equation (20) immediately becomes $\check{\Gamma}^{\rho}{}_{\mu\nu} = \Gamma^{\rho}{}_{\mu\nu}$, and once plugged into equation (18) gives us the Riemann tensor that we are familiar with. Equation (20) also helps us to visualize the definition of our general covariant derivative. Equation (15) can now be written as

$$\mathrm{D}_k A^{i} = \partial_k A^{i} + \left(\Gamma^{i}_{lk} + \check{K}^{i}{}_{lk}\right)A^{l}. \tag{21}$$

This expression roughly means that the general covariant derivative now includes a partial derivative, a parallel transport correction due to curvature, and in addition to that a correction due to torsion.

In the Weitzenböck spacetime, it is defined that the spin connection that is vanishing, namely $A^a{}_{b\mu} = 0$. With this information, we can see straight away that equation (13) gives us $\breve{\Gamma}^\rho{}_{\nu\mu} = h_a{}^\rho \partial_\mu h^a{}_\nu$, equation (16) gives us $\breve{R}^a{}_{b\nu\mu} = 0$, and finally equation (17) gives us $\breve{T}^a{}_{\nu\mu} = \partial_\nu h^a{}_\mu - \partial_\mu h^a{}_\nu$. So from this discussion thus far, we see that the equations for $\breve{\Gamma}^\rho{}_{\nu\mu}$, $\breve{R}^a{}_{b\nu\mu}$ and $\breve{T}^a{}_{\nu\mu}$ are very different in the Riemann and Weitzenböck spacetimes, and they are not to be confused.

The Teleparallel Lagrangian

The Lagrangian density of teleparallel gravity $\mathcal{L}_T$ is defined to be

$$\begin{aligned}\mathcal{L}_T &= \frac{hc^4}{16\pi G} T \\ &= \frac{hc^4}{16\pi G}\left(\frac{1}{4}\breve{T}^\rho{}_{\mu\nu}\breve{T}_\rho{}^{\mu\nu} + \frac{1}{2}\breve{T}^\rho{}_{\mu\nu}\breve{T}^{\mu\nu}{}_\rho - \frac{1}{2}\breve{T}_{\rho\mu}{}^\rho\breve{T}^{\nu\mu}{}_\nu\right)\end{aligned} \tag{22}$$

where $h = \left|h^a{}_\mu\right|$. The first term in equation (22) exists following the rules of the usual Lagrangians of gauge theories, while the next two terms exist due to the fact that the tetrad field enables algebra and spacetime indices change into one another.[11] With some mathematical manipulation, equation (22) can also be re-written as

$$\mathcal{L}_T = \frac{hc^4}{16\pi G}\left(\breve{K}^{\mu\nu\rho}\breve{K}_{\rho\nu\mu} - \breve{K}^{\mu\rho}{}_\mu\breve{K}_{\rho\nu}{}^\nu\right) \tag{23}$$

$$\mathcal{L}_T = \frac{hc^4}{32\pi G}\breve{T}_{\rho\mu\nu}\check{S}^{\rho\mu\nu}. \tag{24}$$

In equation (24), $\check{S}^{\rho\mu\nu}$ is known as the *superpotential*, $\check{S}^{\rho\mu\nu} = \breve{K}^{\mu\nu\rho} - g^{\rho\nu}\breve{T}^{\sigma\mu}{}_\sigma + g^{\rho\mu}\breve{T}^{\sigma\nu}{}_\sigma$.

It is intuitive to ask whether the Lagrangian in teleparallel gravity is equivalent to the Lagrangian in general relativity. In fact, a vigorous mathematical proof is able to show that these two Lagrangians are equivalent up to a divergence term,

$$\mathcal{L}_T = \mathcal{L}_{GR} - \partial_\mu\left(\frac{hc^4}{8\pi G}\breve{T}^{\nu\mu}{}_\nu\right). \tag{25}$$

The divergence term is a surface term, it should vanish when the Lagrangian is integrated through all spacetime,

$$S = \frac{c^4}{16\pi G}\int T\, h\, d^4x. \tag{26}$$

The principle of least action is able to yield the exact same Einstein's field equation as expected.

To summarize this section, teleparallel gravity is formulated on a differential geometrical framework, it works in the Weitzenböck spacetime, it has vanishing curvature but finite torsion, and its Lagrangian is equivalent to the Einstein-Hilbert Lagrangian up to a divergence term. This is the mathematical framework that is needed to study $f(T)$ gravity in section **2.5.2**.

2.4 Comparison of General Relativity and Teleparallel Gravity

2.4.1 Summary Table

The table below summarizes the key conceptual differences between general relativity and teleparallel gravity:

GENERAL RELATIVITY	TELEPARALLEL GRAVITY
Covariant Derivative	
$\nabla_k A^i = \partial_k A^i + \Gamma^i_{lk} A^l$	$\mathrm{D}_k A^i = \partial_k A^i + \left(\Gamma^i_{lk} + \breve{K}^i{}_{lk}\right) A^l$
Connection	
Levi-Civita Connection $\Gamma^\rho_{\nu\mu} = \frac{1}{2} g^{\rho\sigma}\left(\partial_\nu g_{\sigma\mu} + \partial_\mu g_{\sigma\nu} - \partial_\sigma g_{\nu\mu}\right)$	Weitzenböck Connection $\breve{\Gamma}^\rho{}_{\nu\mu} = h_a{}^\rho \partial_\mu h^a{}_\nu$
Curvature Tensor	
$R^\alpha{}_{\beta\gamma\sigma} = \partial_\sigma \Gamma^\alpha_{\beta\gamma} - \partial_\gamma \Gamma^\alpha_{\beta\sigma} + \Gamma^\alpha_{\rho\sigma}\Gamma^\rho_{\beta\gamma} - \Gamma^\alpha_{\rho\gamma}\Gamma^\rho_{\beta\sigma}$	$\breve{R}^\alpha{}_{\beta\gamma\sigma} = 0$
Torsion Tensor	
$T^a{}_{\nu\mu} = 0$	$\breve{T}^a{}_{\nu\mu} = \partial_\nu h^a{}_\mu - \partial_\mu h^a{}_\nu$
Action	
$S = \int \left(\frac{c^4}{16\pi G} R + \mathcal{L}_M\right) \sqrt{-g}\, d^4x$	$S = \int \left(\frac{c^4}{16\pi G} T + \mathcal{L}_M\right) h\, d^4x$

Table 1: Comparison of General Relativity and Teleparallel Gravity

2.4.2 Why Teleparallel Gravity?

Studying teleparallel gravity requires a lot of hard work: one needs to have sufficient knowledge in differential geometry and Lie algebra to understand the equations and to get a clearer picture of the theory. A natural question to ask would be, 'why study teleparallel gravity?' It turns out that teleparallel gravity has a lot of advantages and interesting points that made it worth discovering.

Firstly, teleparallel gravity welcomes back the picture of 'force' through the contorsion tensor, and it shows up as a gauge theory just like other forces like electromagnetism. As said earlier, general relativity uses the geodesic equation, which is a concept unique to its own. The existence of the geodesic equation causes a lot of inconsistencies if one attempts to unite gravitation with other forces, as the spin connection that general relativity works in has made gravitation and inertial effects mixed together.[10] With that, it is impossible to write down an energy-momentum tensor for gravitation without inertia contributing. In fact, this was the reason why Møller resolved to teleparallelism in the first place.

Secondly, the gauge description of teleparallel gravity remains a consistent theory in the absence of universality. Teleparallel gravity is consistent with the strong equivalence principle, but at the same time is valid even without it. It does not violate the $U(1)$ gauge invariances of electromagnetism.[11] Thus we can see that teleparallel gravity provides a better framework than general relativity to resolve the unification of gravitation and quantum mechanics, since the equivalence principle in which general relativity holds strongly onto cannot co-exist with the uncertainty principle. This allows many existing conflicts to be solved: spin-2 fields can be coupled to gravitation, and gravitation can be quantized using the mathematical framework of teleparallel gravity.[11]

Most important of all, teleparallel gravity is an easier environment to work with when it comes to explaining the accelerating universe. In general relativity, $f(R)$ gravity models are one of the many attempts made to act as an alternative to the cosmological constant. However, it produces 4^{th} order equations and 2^{nd} derivatives which are hard to work with, and it also suffers from weak field tests, gravitational instabilities, and it doesn't determine a matter dominated era previous to the accelerating era.[14] $f(T)$ gravity models however, are only 2^{nd} order equations with up to 1st derivatives, they are easier work with and calculate. The mathematics of $f(R)$ and $f(T)$ gravity will be explained in sections **2.5.1** and **2.5.2**.

All in all, despite the difficulty to understand the theory, teleparallel gravity seems to have many implications on our current efforts to unite forces and to resolve inconsistencies between them. Currently there is no new known physics of torsion. A suggestion was that there might be new physics in neutron stars, since the alignment of neutrons might produce a macroscopic spin, and consequently a torsion field.[10] However, since the physics of neutron stars is well understood with general relativity, and that teleparallel gravity is just an alternative view of it, we shouldn't expect anything new to arise from it. Teleparallel gravity, in the words of Arcos, is a "new way to look at all gravitational phenomena, including those shaping the universe itself".[11] Many current gravitational phenomena (like gravitational lensing) may have a different interpretation using teleparallel gravity, and thus studying this theory would definitely be worth the time. We should not rule out the possibilities of finding new motivations for experiments, or even new physics through the understanding of teleparallel gravity.

2.5 The Accelerating Universe

Physicists have long known that the universe is expanding since the days of Hubble, when he first realized that galaxies and stars are moving away from one another, and he suggested his famous Hubble constant. Yet it wasn't until the recent 1998 when Saul Perlmutter and group found out that the universe is not only expanding, but at an accelerating rate.[5] The fact that the universe is not static has baffled many, and modifications had to be made to Einstein's equation to account for this expanding universe.

Let us revisit the FLRW metric (equation (2)) and Einstein's field equation (equation (20)). To know how the universe expands and accelerates, we need to study the scale factor $a(t)$. Assuming a homogeneous, isotropic and a perfect-fluid-dominated universe ($T_{00} = -\rho, T_{ii} = P$), we plug equation (2) into equation (20) and we get two independent equations known as the *Friedman equations*:

$$2\frac{\ddot{a}}{a} + \frac{\dot{a}^2 + kc^2}{a^2} = -\frac{8\pi G}{c^2}P \tag{27}$$

$$3\frac{\dot{a}^2 + kc^2}{a^2} = \frac{8\pi G}{c^2}\rho. \tag{28}$$

Here P and ρ are the pressure and the energy density of the fluid. Plugging equation (28) into equation (27), we get

$$\frac{\ddot{a}}{a} = -\frac{4\pi G}{c^2}\left(P + \frac{\rho}{3}\right). \tag{29}$$

For a universe to accelerate, The second derivative of $a(t)$, $\ddot{a}$ has to be positive. If we assume that the universe is flat ($k = 0$), we find that the equation must satisfy the condition $w = \frac{P}{\rho} < -\frac{1}{3}$, in which we define w to be the *equation of state*. It is easy to see that a matter or radiation dominated universe cannot cause an accelerating universe. If we analyze the energy-stress tensor, we will see that dust (or slow moving matter in general) has $w = 0$, since $P \ll \rho$ for dust. On the other hand, relativistic matter (or radiation in general) has $w = \frac{1}{3}$, as the radiation pressure is $\frac{1}{3}$ of its density due to the randomization of photons in all directions.[15] Therefore, we see that a universe dominated by matter or radiation alone cannot make the universe expand: the electromagnetic and gravitational forces could only create a decelerating universe.

To explain the accelerating universe, we need to either introduce a new substance that has negative pressure $\left(w < -\frac{1}{3}\right)$, or we make a modification to the gravity theories, or we make a modification on matter. The following subsections will briefly explain the current approaches to solve the problem from the general relativity and the teleparallel gravity point of view.

2.5.1 The Approach from General Relativity

There are in fact many ways to explain the accelerating universe, but to ensure that the discussions are closely related to this work, Only 2 methods will be discussed, and they are the cosmological constant and the $f(R)$ gravity model.

Cosmological Constant

In order to explain the cosmic acceleration, some physicists suggested the existence of a new form of substance called the dark energy. This dark energy should have a negative pressure and equation of state $w \leq -\frac{1}{3}$ in order that the universe expands at an accelerating rate.

One of the possible representations of dark energy is the cosmology constant Λ. Initially Einstein introduced the cosmological constant so that he can explain a static universe. However, his efforts failed because firstly the static equilibrium he suggested was unstable, and secondly because now we know that the universe isn't static at all. The same cosmological constant used by Einstein is now resurrected and used with a new interpretation. Therefore equation (20) with the addition of the cosmological constant now becomes

$$R_{\mu\nu} - \frac{1}{2} g_{\mu\nu} R + g_{\mu\nu}\Lambda = \frac{8\pi G}{c^4} T_{\mu\nu}. \qquad (30)$$

Here the term $g_{\mu\nu}\Lambda$ is the dark energy substance that we introduced. This cosmological model with the added constant term is known as the Lambda Cold Dark Matter (ΛCDM) model. Writing it in terms of a energy-momentum tensor (subscript DE means dark energy),

$$g_{\mu\nu}\Lambda = \frac{8\pi G}{c^4} T_{\mu\nu,DE} \tag{31}$$

we get $\rho_{DE} = \frac{\Lambda c^4}{8\pi G} = -P_{DE}$, and thus $w = -1$. So if we assume a matter-dominated universe (subscript m) with the presence of dark energy, the Friedman equations become

$$2\frac{\ddot{a}}{a} + \frac{\dot{a}^2 + kc^2}{a^2} + \frac{8\pi G}{c^2} P_{DE} = 0 \tag{32}$$

$$3\frac{\dot{a}^2 + kc^2}{a^2} - \frac{8\pi G}{c^2}\rho_{DE} = \frac{8\pi G}{c^2}\rho_m \tag{33}$$

and if we put equation (33) into equation (32), we see that

$$\frac{\ddot{a}}{a} = \frac{4\pi G}{3c^2}(2\rho_{DE} - \rho_m). \tag{34}$$

This means that a positive acceleration is possible if the percentage of dark energy is more than half the percentage of matter. In fact, dark energy models suggest that the universe is filled with 28% matter and 72% dark energy, thus proving that the cosmological constant is a viable method to prove that the universe expands at an accelerating rate.

The usual method to test this theory is to assume that w_{DE} is arbitrary, and we use various observational constraints to fit and find the best fit value of w_{DE} and $\Omega_{m,0}$, the current density of matter in the universe. Others have also proposed a time or redshift-dependent w_{DE} too. Kowalski et al used observational constraints from the type 1a supernova, cosmic microwave background and the baryonic acoustic oscillation test to obtain values of $(\Omega_M, w_{DE}) = (0.265^{+0.022}_{-0.021}, -0.955^{+0.060}_{-0.066})$, which showed that our universe favours a model with dark energy.[16]

$f(R)$ Gravity Models

$f(R)$ gravity models are considered as modified gravity models, where the gravitation laws of general relativity are modified to explain the accelerating universe. The basic principle behind it is to make the substitution $R \to f(R)$, where $f(R)$ means 'function of R', with R being the Ricci Scalar. In this case, we make a modification of the Einstein-Hilbert action equation (9) into

$$S = \int \frac{c^2}{8\pi G} f(R)\sqrt{-g} + \mathcal{L}_M \; d^4x. \tag{35}$$

Varying the action with respect to $g_{\mu\nu}$, and taking the trace of it, we get two equations below,[17]

$$f'(R)R_{\mu\nu} - \frac{1}{2}f(R)g_{\mu\nu} - \nabla_\mu\nabla_\nu f'(R) + g_{\mu\nu}\Box f'(R) = \frac{8\pi G}{c^2}T_{\mu\nu} \tag{36}$$

$$3\Box f'(R) + f'(R)R - 2f(R) = \frac{8\pi G}{c^2}T \tag{37}$$

where $f'(R) = \frac{\partial f}{\partial R}$, $T = g^{\mu\nu}T_{\mu\nu}$ and $\Box$ is the D'Alembertian operator. Assuming a flat FLRW universe, equation (36) and (37) can be simplified to become

$$3f'(R)H^2 = \frac{8\pi G}{c^2}\rho_m + \frac{f'(R)R - f(R)}{2} - 3H\dot{f}'(R) \tag{38}$$

$$2f'(R)\dot{H} = -\frac{8\pi G}{c^2}\rho_m - \ddot{f}'(R) + H\dot{f}'(R). \tag{39}$$

These equations which related H, the Hubble parameter with the $f(R)$ functions are required for observational test fittings. Equations (38) and (39) simply mean that as long as we can find a suitable $f(R)$ function with a few variable parameters, after fitting it with data from an observational test, we will be able to conclude whether it is a good alternative to the cosmological constant or not, provided that the function has no stability issues. However, the $f(R)$ functions chosen are not arbitrary, they need to fulfill certain conditions. Let R_0 be the curvature at the present time, we need[17]

1. $f'(R_0) > 0$ at $R \geq R_0$, for the stability of cosmological perturbations;
2. $f''(R_0) > 0$ at $R \geq R_0$, to avoid anti-gravity, or avoiding gravitons turning into ghosts (degrees of freedom with kinetic energy terms with the 'wrong' sign[18]);
3. $f(R) \Rightarrow R - 2\Lambda$ at $R \gg R_0$, the model should revert to ΛCDM model at high density;
4. $0 < R\frac{f''(R)}{f'(R)} < 1$ at the de Sitter point (a point which corresponds to a vacuum solution and R is constant[17]), satisfying $Rf'(R) = 2f(R)$.

The following are two of the many $f(T)$ gravity models that satisfy the above requirements:

$$f(R) = R - \mu R_c \frac{\left(\frac{R}{R_c}\right)^{2n}}{\left(\frac{R}{R_c}\right)^{2n} + 1} \tag{40}$$

$$f(R) = R - \mu R_c \left[1 - \frac{1}{\left(1 + \frac{R^2}{R_c^2}\right)^n}\right]. \tag{41}$$

In these models, R_c are constants, while μ and n are varying parameters to be found through observational constraints. A best fit value of n or μ could be found by conducting χ^2 tests against various observational data, and the lower the χ^2 the better the model fits the observational data.

$f(R)$ gravity models have many implications, interpretations and aspects that could be studied. Its observational signatures, its local gravity constraints, the different transformational approaches (like the Palatini formalism) are just a few of the many things that one could study about this theory. In fact, $f(R)$ gravity models are not entirely flawless: many of these $f(R)$ models have problems like matter instability, the absence of matter era, or have conflicts with the standard model of particle physics. Most of the time, $f(R)$ functions are required to be made such that their deviation from the ΛCDM model must be small.[17] But practically, $f(R)$ gravity models involve 4th-order equations, and thus making the entire fitting process tedious.

Other Approaches

Besides the cosmological constant and the $f(R)$ gravity theory, there are many other approaches to explain the accelerating universe. There is a group of theories know as the modified matter models, where they have included exotic matter sources in the energy-momentum tensor which possess negative pressure. Such models are like quintessence (canonical scalar field), k-essence (scalar fields with non-canonical kinetic terms), coupled dark energy with dark matter models and etc.[17] There is also another group of theories known as the modified gravity models, in which $f(R)$ gravity is just one of it. Examples of other modified gravity models are the Gauss-Bonnet dark energy model (extension of $f(R)$ gravity), scalar-tensor theories (R coupled to a scalar field) and the Dvali-Gabadadze-Porrati (DGP) model (a braneworld in 5 dimensions).[17]

Lastly, there are also methods that one could explain cosmic acceleration without dark energy. These methods include inhomogeneities in the distribution of

matter, the presence of underdensed bubbles (void model) and the back-reaction of cosmological perturbations.[17] In summary, there are a lot of approaches to explain the accelerating universe, and researches are continuously being done in order to fit these cosmological models with observational data, to affirm their viability and validity.

2.5.2 The Approach from Teleparallel Gravity

As the research on teleparallel gravity is fairly recent, there are not as many methods in teleparallel gravity to explain the cosmic acceleration as compared to general relativity, although every model in general relativity should have a teleparallel equivalent. In this section, $f(T)$ gravity will be introduced, and this will be the gravity model used for this project.

$f(T)$ Gravity

Also known as torsion gravity, this model looks very similar to $f(R)$ gravity, as it too involves the change in action, but in this case $T \to f(T)$. T is the torsion scalar, it is also the component of the teleparallel Lagrangian. The teleparallel action (equation (26)) now takes the form

$$S = \int \left[\frac{c^4}{16\pi G} f(T) h + \mathcal{L}_M \right] d^4x \tag{42}$$

where $\mathcal{L}_M$ is the matter component of the Lagrangian. Using the principle of least action ($\delta S = 0$) in variation with the tetrad, we arrive at

$$S_i{}^{\mu\nu} \partial_\mu T f''(T) + \left[e^{-1} \partial_\mu \left(e S_i{}^{\mu\nu} \right) - e_i^\lambda T^\rho{}_{\mu\lambda} S_\rho{}^{\nu\mu} \right] f'(T) + \frac{1}{4} e_i^\nu f(T) = 4\pi G e_i{}^\rho T_\rho{}^\nu. \tag{43}$$

This equation may look intimidating, but simplifications can be done. We assume a flat homogeneous and isotropic FLRW universe, our teleparallel Lagrangian (equation (24)) magically simplifies to $T = -6H^2$, where H is the Hubble parameter. If we substitute this new information into equation (43), and taking the 00 and ii components (proof omitted), we arrive at our modified Friedman equations:

$$12H^2 f'(T) + f(T) = \frac{16\pi G}{c^2} \rho \tag{44}$$

$$48\dot{H}H^2 f''(T) - 4\left(\dot{H} + 3H^2\right) f'(T) - f(T) = \frac{16\pi G}{c^2} p. \tag{45}$$

When compared these equations to equations (38) and (39) of $f(R)$ gravity, one can easily see that this set of equations is much easier to handle. They are at maximum 2nd-order equations and are easier to manipulate. Equation (44) will be the starting

point of this project: when a new $f(T)$ is formulated, it will be plugged into equation (44) and an equation of H in terms of the other variables will be produced. With this equation, we will fit it to the observational constraints / data, which will be explained in **Chapter 3**. The $f(T)$ function introduced, like those in $f(R)$ theories, should contain at least one free parameter, whereby it could be varied and find a best fit value for it when fitted to observational χ^2 tests. As for the conditions for proposing a viable $f(T)$ function, this will be discussed in **Chapter 4**.

An important note here is that $f(T)$ gravity might have stability issues, or some unforeseen problems that might arise when using certain arbitrary functions, just like $f(R)$ gravity. Ong and group have noted that $f(T)$ gravity might suffer problems in time propagation and evolution.[19] Keisuke also pointed out that one has to conduct non-linear analysis on $f(T)$ gravity to ensure that it has no stability issues.[2] But this project assumes that there are no fatal issues arising from this model which would render this model obsolete. For future work, it is suggested that the other aspects of $f(T)$ gravity be looked into to ensure the validity of this model.

Another note would be that the modified models we have seen thus far are metric dependent, and they assume a flat, homogeneous and isotropic FLRW universe. This unavoidable assumption has to be taken in order to proceed to simplify many calculations. In fact, it isn't much of a danger since this metric still fits our current observable universe the best. There are other metric independent studies (like cosmography) which explain the cosmic acceleration, but it will be beyond the scope of this thesis.

Chapter 3

THE OBSERVATIONAL CONSTRAINTS

3.1 Overview

In order to prove that our theory is consistent with observations, we need to conduct observational tests to constrain our model. In our case, $f(T)$ models with one free parameter are suggested, and once these $f(T)$ models are substituted into equation (44), we will get an equation of $H(z)$, and it will plugged into various equations used in the following observational tests, so that their theoretical values will be compared with those data observed. In the following section, 5 kinds of observational tests will be discussed, they are the type Ia supernovae, cosmic microwave background, baryonic acoustic oscillation, observational Hubble data and gamma-ray bursts. Of these 5 observational constraints, only the first 4 tests would be used to constrain the $f(T)$ functions. The reasons for not including the gamma-ray bursts test will be explained in section **3.6**.

3.2 Type Ia Supernovae

A supernova is a stellar explosion, a cataclysmic nuclear explosion in stars. Generally stars that have masses greater than $8M_{\odot}$ continue to heat up and undergo mass loss and gas depletion up till a certain point where its core suddenly collapses due to degeneracy pressure and photodisintegration. The super red giant star will then explode to form a supernova. Supernovae are very luminous objects which sometimes outshine an entire galaxy, but will later fade off slowly with time.

Type Ia Supernovae (SNE Ia) are supernovae that do not contain hydrogen, and presents a singly ionized silicon (Si II) line at 615nm near peak light.[20] Unlike normal supernovae, SNE Ia are said to occur in binary star systems, in which one star is a white dwarf, and the other a bigger star. In simple words, the gas from the bigger star is spilled to the white dwarf, and the white dwarf explodes as it reaches its critical mass, forming an SNE Ia. The detailed formation process of an SNE Ia is explained in **Fig. 2.**

Since all SNE Ia explosions occur at almost the same condition, the luminosity-time relation of the SNE Ia is said to follow a characteristic light curve, in which the peak of the curve is quite consistent at a value of absolute magnitude $M = -19.3$. Therefore,

SNE Ia have been used by many astronomers as *standard candles* to determine intergalactic distances.

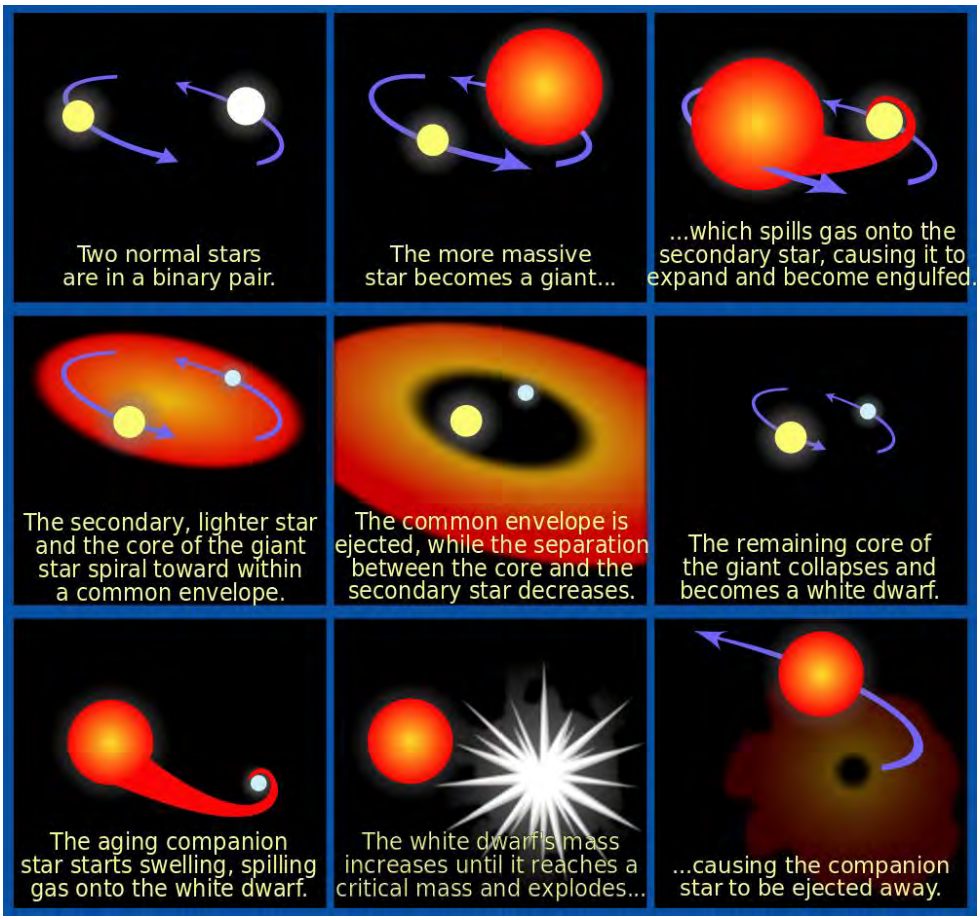

Fig. 2: The Progenitor of a Type 1a Supernova[21]

One way to measure intergalactic distances is to measure the luminosity of a distant object. The luminosity distance of a supernova is defined to be

$$d_L^2(z) = \frac{L}{4\pi F}, \tag{46}$$

where L is the absolute luminosity of the supernova, and F being the radiant flux at that point. Assuming a flat FLRW metric, the luminosity and radiant flux of the supernova has been calculated to be[22]

$$L = L_0(1+z)^2 \tag{47}$$

$$F = \frac{L_0}{4\pi a_0^2 r^2} \tag{48}$$

where r is the coordinate of space, and L_0 is the luminosity of the SNE Ia at $r = 0$. z is the redshift of the SNE Ia, and z is related to the scale factor through the equation

$$1 + z = \frac{a_0}{a} \tag{49}$$

where a_0 is the scale factor at the current time. The redshift of a celestial object is positive if the universe is expanding away from the observer, thus in an accelerating universe, we expect to see further high-redshift galaxies to be much fainter than galaxies nearer to us.

Plugging equations (47) and (48) into (46), we get

$$d_L(z) = a_0(1 + z)r. \tag{50}$$

Now using the properties of a light-like geodesic, $-c^2dt^2 + a^2(t)dr^2 = 0$, equation (50) will turn into

$$d_L(z) = a_0(1 + z)\int_0^r d\tilde{r} = a_0(1 + z)\int_{t_1}^{t_0} \frac{c}{a(t)}dt. \tag{51}$$

By taking the time derivative on both sides for equation (49), we could use this relation to modify equation (51) into

$$d_L(z) = c(1 + z)\int_0^z \frac{1}{H(\tilde{z})}d\tilde{z}. \tag{52}$$

This is the luminosity distance of SNE Ia, in terms of its redshift and the Hubble parameter. Therefore if we can derive an expression of $H(z)$ from our proposed $f(T)$ gravity models, we can substitute the equation into this expression to find the luminosity distance of a SNE Ia given its redshift.

The luminosity distance of a supernova can be measured only indirectly through the measurement of the distance modulus μ_B, which is a difference between its absolute magnitude ($M = -19.3$) and its maximum apparent magnitude $m_B^{\max}$. μ_B is defined to be

$$\mu_B = |m - M| = 5\log\left(\frac{d_L}{10}\right). \tag{53}$$

d_L is measured in parsecs (pcs), while the units of H in this expression is in m s^{-1} pc^{-1}. If we want H to be measured in km s^{-1} Mpc^{-1}, equation (53) can be re-written as

$$\mu_B = 5\log\left[100c(1 + z)\int_0^z \frac{1}{H(\tilde{z})}d\tilde{z}\right] \tag{54}$$

Experimentally, the redshift of the supernova can be obtained by spectrometry, and the distance modulo is obtained by observing the apparent magnitude of a supernova and fitting it to the characteristic lightcurve. So the observed value of distance modulo could be compared with the theoretical value obtained from a particular model, and if we want to find the best fit model, the difference between these values should be as small as possible. The Supernova Cosmology Project (SCP) has compiled its latest dataset (Union2.1) which contains the distance modulo, redshift and uncertainty for 580 observed supernovae over many years,[23] and these data will be used to conduct a χ^2 fit for the various $f(T)$ models.

3.3 Cosmic Microwave Background Radiation

Cosmic microwave background (CMB) is the thermal radiation filling the observable universe. It is explained by many cosmologists that the CMB is the radiation left over from the early stage of the universe, and is a proof to the existence of a Big Bang. The spectrum of radiation measured by the COBE satellite has a temperature of 2.735±0.06 K, which is shown to have anisotropic properties[5]. The spectrum of the CMB follows a blackbody curve, which peaks at microwave regions.

The anisotropy of the CMB temperature is said to be affected by the acceleration of the universe, and this situation leads to a linear shift in position of acoustic peaks. We first define the sound horizon r_s, the radius of a shell of baryonic matter moving outwards from the centre of the Big Bang after the decoupling epoch where the photons no longer interact with matter. r_s can be represented by the formula below:

$$r_s(\eta) = \int_0^{\eta} c_s(\tilde{\eta})\, d\tilde{\eta} \tag{55}$$

where η is the distance travelled by the sound, which can also be represented as $d\eta = \frac{1}{a}dt$, and a being the scale factor. c_s is the speed of sound, which can be represented by the equation[17]

$$c_s = \frac{1}{\sqrt{3(1+R_s)}} = \frac{1}{\sqrt{3\left(1+\frac{3\rho_b}{4\rho_\gamma}\right)}} \tag{56}$$

where ρ_b and ρ_γ are the energy densities of baryons and photons respectively. Next, the CMB acoustic peaks can be represented by the formula

$$\theta_A = \frac{r_s(z_{dec})}{d_A^{(c)}(z_{dec})} \tag{57}$$

where $d_A^{(c)}(z_{dec})$ is the commoving angular diameter distance evaluated at z_{dec}, which is the redshift at the decoupling epoch (estimated value, $z_{dec} \approx 1090$),

$$d_A^{(c)}(z_{dec}) = \frac{d_L(z_{dec})}{1 + z_{dec}} = c \int_0^{z_{dec}} \frac{1}{H(\tilde{z})} d\tilde{z}. \tag{58}$$

Once again assuming a flat universe, the CMB multipole l_A that corresponds to the angle θ_A can be written as

$$l_A = \frac{\pi}{\theta_A} = \frac{\pi c}{r_s(z_{dec})} \int_0^{z_{dec}} \frac{1}{H(\tilde{z})} d\tilde{z}. \tag{59}$$

With the expression r_s calculated by Hu et al[24], the multipole can be written as

$$l_A = \frac{3\pi}{4} \sqrt{\frac{\Omega_{b,0}}{\Omega_{\gamma,0}}} \left[\ln \left(\frac{\sqrt{R_s(a_{dec}) + R_s(a_{eq})} + \sqrt{1 + R_s(a_{dec})}}{1 + \sqrt{R_s(a_{eq})}} \right) \right]^{-1} \mathcal{R} \tag{60}$$

where a_{dec} and a_{eq} are the scale factors at decoupling epoch and the radiation-matter equality respectively, and $\Omega_{b,0}$ and $\Omega_{\gamma,0}$ are the baryon and photon density at current time.

The expression $\mathcal{R}$,

$$\mathcal{R} = \sqrt{\Omega_{m,0}} H_0 c \int_0^{z_{dec}} \frac{1}{H(\tilde{z})} d\tilde{z} \tag{61}$$

is known as the CMB shift parameter, it relates the angular diameter distance to the last scattering surface with the angular scale of the first acoustic peak in the CMB power spectrum. The change in cosmic expansion history from the decoupling epoch to the present day affects the CMB shift parameter, which in turn shifts the multipole. The Wilkinson Microwave Anisotropy Probe (WMAP) 5-year bound on CMB shift is measured to be $\mathcal{R} = 1.710 \pm 0.019$, and thus for a theoretical value of $\mathcal{R}$ calculated from $f(T)$ gravity models, we can fit and compare it to this value.[17]

The CMB data do not provide a tight constraint on dark energy, because firstly it depends weakly on w_{DE}, and secondly, the CMB data tabulated by WMAP is highly dependent on the ΛCDM model.[25] Thus, the CMB test is normally constrained together with the SNE observations.

3.4 Baryonic Acoustic Oscillation

Baryonic Acoustic Oscillation (BAO) is the regular periodic fluctuation in the density of the visible baryonic matter. It is caused by acoustic waves which existed in the early universe. Baryons are strongly coupled to photons before the decoupling epoch, so the oscillation of sound waves is imprinted in baryon perturbations. The case is similar to CMB anisotropy, but this phenomena is originated from the drag epoch instead of the decoupling epoch. The drag epoch is the time which the baryons are released from the Compton drag of the photons, while the decoupling epoch happened earlier, it is the time when the photons are able to travel far without being scattered or absorbed by baryons.[26] BAO matter clustering can act as a *standard ruler* in cosmology, which means that its size is known, and we can determine its distance from earth by measuring its apparent angular diameter alone.

Similar to CMB, we define the sound horizon r_s here, but this time at $z = z_d \approx 1020$, the redshift at the drag epoch:

$$r_s(z_d) = \int_0^{\eta_d} c_s(\tilde{\eta})\, d\tilde{\eta}. \tag{62}$$

$r_s(z_d)$ is estimated by Eisenstein and Hu to be about 150Mpc.[27] Next, we introduce what we are able to observe: the angular and redshift distributions of galaxies as power spectra. We are able to measure two ratios: θ_s which characterizes the angle orthogonal to the line of sight, and δ_s which characterizes the oscillations along the line of sight.[17] These two ratios are formulated as follows:

$$\theta_s(z) = \frac{r_s(z_d)}{d_A^{(c)}(z)}, \qquad \delta z_s(z) = \frac{r_s(z_d)H(z)}{c} \tag{63}$$

where $d_A^{(c)}(z)$ here is the commoving angular diameter distance, it is related to the proper angular diameter distance d_A by the equation $d_A^{(c)} = \frac{d_A}{1+z}$. These two ratios are not observed independently, but instead measured together through the effective distance ratio r_{BAO}, observed from the spherically average spectrum,

$$r_{BAO}(z) = \left[\frac{\theta_s^2(z)\delta z_s(z)}{z}\right]^{\frac{1}{3}} = \frac{r_s(z_d)}{D_V(z)} \tag{64}$$

where $D_V(z)$ is defined to be,

$$D_V(z) = c\left[\frac{z}{H(z)}\left(\int_0^z \frac{d\tilde{z}}{H(\tilde{z})}\right)^2\right]^{\frac{1}{3}}. \tag{65}$$

BAO is detected in a spectroscopic sample of luminous red galaxies (LRG) by the Sloan Digital Sky Survey (SDSS). The combined data obtained from the 2-degree Field (2dF) Galaxy Redshift Survey and SDSS measured r_{BAO} at two distinct redshifts, and their values are $r_{BA0}(0.2) = 0.1905 \pm 0.0061$ and $r_{BAO}(0.35) = 0.1097 \pm 0.0036$.[17] With these observed values, we can use equation (64) to compare the theoretical value with them for model fitting. The BAO test is seen as a powerful low-redshift probe, as it is limited by statistical uncertainties rather than systematic.[28] Although a tighter constraint than CMB, BAO tests are still much weaker than SNE tests, and should be constrained together with SNE and BAO for a better effect.

3.5 Observational Hubble Data

The observational Hubble data (OHD) is based on the differential ages of passively evolving galaxies.[29] The measure of differential ages is more reliable than the measure of the absolute ages of galaxies itself, since it is not vulnerable to systematic uncertainties.[30] Consider a cluster of galaxies, by using equation (49) and the fact that $H(z) = \frac{1}{a(t)}\frac{da(t)}{dt}$, we get

$$H(z) = -\frac{1}{1+z}\frac{dz}{dt} \tag{66}$$

Here $\frac{dz}{dt}$ is the differential age of the galaxy. Thus if we have a value for $\frac{dz}{dt}$, we are able to find an expression for the Hubble parameter. $\frac{dz}{dt}$ is obtained by taking a data pool of galaxies and calculate their relative changes in redshifts Δz and then divided by their relative ages Δt.

The finding of differential ages of galaxies involves the binning of groups of galaxies together, and sophisticated statistical methods are used to interpolate their relative redshifts and ages. The Hubble data obtained by Stern et. al for example, is through the analysis of high-quality spectra with the Keck-LRIS spectrograph of red-envelope galaxies in 24 galaxy clusters in the redshift range $0.2 < z < 1.0$ from the

Spectroscopic, Photometric, Infrared-Chosen Extragalactic Survey (SPICES) and the VIMOS VLT Deep Survey (VVDS).[31] After the analysis, they tabulate an output of several H values with their corresponding z and uncertainties. These $H(z)$ values obtained will be used for model fitting.

The advantage of using OHD to constrain cosmological models over constraints like SNE, CMB and BAO is that it does not involve integration. In fact, SNE, CMB and BAO tests depend on studying the integral of the expansion history, rather than the expansion history itself, and OHD is able to circumvent this limitation.[31] The OHD constraint is a relatively new concept, and researches are ongoing to improve the current data set.

3.6 Gamma Ray Bursts

Gamma-ray bursts (GRBs) are flashes of gamma-rays associated with explosions that are extremely energetic. Cosmic gamma-rays were accidentally discovered during the 1960s, when the United States sent two satellites into space to detect nuclear weapon experiment activities.[32] Gamma-ray flashes can be detected by densely packed crystal blocks as they have wavelengths with magnitudes of atomic distances.[33] Gamma rays possess energies greater than 100keV, and they are classified as the brightest electromagnetic waves observed in the universe. The flashes range from 10ms to a few minutes, and they usually have an afterglow at longer wavelengths. The shorter GRBs tend to appear far from active regions of galaxies, while the longer ones appear in star-forming galaxies where core-collapse of massive young stars are common.[34]

Although discovered 50 years ago, vigorous researches on gamma-ray sources have only started in 1991 due to the limitation of instrumentation.[32] The progenitor of GRB is currently still unknown, but some suggested that they originated from supernovae, hypernovae, neutron stars, pulsars and black holes.[33] Physicists have tried to identify candidate objects from the direction of GRBs, but usually end up not seeing anything, thus making them suggest that GRBs are originated from the very distant galaxy about billions of lightyears away, too faint to be seen.

Currently it is impossible to conduct a one-on-one GRB to theoretical value χ^2 fit, because the physics of GRBs is not well understood, furthermore the dataset of GRB with low redshifts are insufficient. The only way to use GRBs as an observational constraint currently is to use statistical methods of correlation. There are various correlation methods used, but the most popular one would be the Amati's correlation. Amati uses the $E_{peak} - E_{iso}$ correlation, where E_{peak} is the cosmological rest-frame

spectral peak energy of the GRB, and E_{iso} is the isotropic energy of the GRB. E_{iso} can be related with the luminosity distance through the following relation:[34]

$$E_{iso} = \frac{4\pi d_L^2(z)}{1+z} F. \tag{67}$$

Here F is the flux of the GRB measured. It is important to note that equation (67) is model dependent: it is derived based on the ΛCDM model. This equation tells us that with the measured E, F and z from the GRBs, we are able to map it to $d_L(z)$, which is something that we can compare and study.

Wang proposed a method to use GRB to conduct the observational constraint on cosmological models.[35] Based on Amati's correlation, Wang defined a model independent distance measurement $\bar{r}_p(z)$,

$$\bar{r}_p(z) = \frac{r_p(z)}{r_p(z_0)} \tag{68}$$

where $r_p(z)$ is defined to be

$$r_p(z) = \frac{\sqrt{1+z}}{z} \int_0^z \frac{H_0}{H(\tilde{z})} d\tilde{z}\,. \tag{69}$$

The integral in equation (69) is the same integral seen in the luminosity distance relation. Here z_0 is a reference smallest redshift of the GRBs, and the fraction quantity $\bar{r}_p$ is taken so that the value of H_0 is cancelled out. $\bar{r}_p(z)$ is not something measured directly from the GRB dataset, it is calibrated through a set of equations relating many variables (luminosity, total energy, time lag etc)[35] and later correlated with SNE, CMB and BAO data. Wang himself turned the data of 69 GRBs, into 6 sets of $(\bar{r}_{p,obs}, z_{obs}, \sigma_{\bar{r}_{p,obs}})$ data that could be used to fit cosmological models. Thus, to fit a modeled equation $\bar{r}_{p,theo}$ with $\bar{r}_{p,obs}$, a χ^2 test can be conducted, with the value of χ^2 expressed as follows:

$$\chi^2 = \left(\bar{r}_{p,obs} - \bar{r}_{p,theo}\right)^T C^{-1} \left(\bar{r}_{p,obs} - \bar{r}_{p,theo}\right) \tag{70}$$

Here C is the normalized covariance matrix, $C = \sigma_i \sigma_j \bar{C}_{ij}$, and $\bar{C}_{ij}$ is the correlation matrix computed from the statistical analysis, and σ is the error for the observed values.

Currently the GRB test is not a reliable observational constraint for cosmological models, and the reasons are as follows. Firstly, its physics is still unknown, and thus the

validity of GRB as a *standard candle* is still debatable. Secondly, the test is model dependent, Amati's correlation yields a circularity problem, whereby we have already assumed a cosmology before we fit it.[36] Besides, Wang's 6 sets of data yields results that are 2σ away from the results of Schaefer and also Xu[37], which both use similar methods but having different bins, showing inconsistencies in results. Lastly, the GRB test is a very weak test: it produces a very wide χ^2 contour, it does not affect the results obtained significantly,[29] and it constrains data very weakly.

Therefore, the GRB test although thoroughly studied and discussed in this thesis, it will not be used to constrain the $f(T)$ models proposed in the next chapter. However, the GRB test was still conducted, and its results are included in **Appendix B3** for the interest of the reader.

Although the GRB test has many disadvantages, it still has some advantages over other tests, and might be a very promising observational constraint in the future. Firstly, GRBs have redshifts of $1 < z < 8$, which are in between the redshifts of the SNE ($z < 2$) and the CMB ($z \approx 1090$). Once well understood, it could act as a bridge between both tests, marking a possibility of a general relation between d_L and z. Secondly, while SNE requires the need to subtract dust extinction[36] (in which a model needs to be setup), GRB does not need to, as its radiation is highly penetrative. Lastly, the data of GRBs recorded is currently very low, but is constantly increasing. With more GRBs with lower redshifts detected, d_L could be better calibrated. But due to the long afterglow of the GRBs, data collection might progress quite slowly, and it might be a decade before GRBs become good observational constraints.

Chapter 4

METHODOLOGY

4.1 Objectives

In **Chapter 2**, the theory of teleparallel gravity was discussed, and it was explained how this theory could be modified into $f(T)$ gravity to explain the accelerating universe. In **Chapter 3**, the various observational constraints on the proposed $f(T)$ functions have been discussed too. With sufficient knowledge at hand, this is an appropriate time to explain the *objectives* of this project, and the methodologies used.

The aim of this project is to formulate 3 different forms of $f(T)$ functions with 2 free parameters (α and n) using the various constraints and rules required, obtain a modified Friedman equation from each of them, find $H(z)$ (Hubble parameter as a function of redshift), and then test them with 3 observational tests (SNE, Combined CMB/BAO and OHD test) by using a χ^2 contour plot. The best fit values of $\Omega_{m,0}$ (the current matter density parameter of our universe) and n (one of the free parameters) will be taken at the point with the lowest χ^2 value. These best fit values, the shape of the contour plot produced, and the different results from the different observational constraints will be compared to the ΛCDM model. Discussion on the viability and validity of the $f(T)$ functions will be brought forward too.

In the following sections, the discussion will focus on the 3 $f(T)$ functions that will be proposed: the equations involved, the construction method, and the $H(z)$ equation that will be derived from it. Sections **4.3** to **4.5** will be a discussion of the mathematics behind the χ^2 tests for the 3 observational constraints, the bisection method and the Gauss-Legendre Quadrature.

4.2 $f(T)$ Functions

4.2.1 Constraints on $f(T)$ Functions

We recall the action for $f(T)$ gravity,

$$S = \int \frac{hc^4}{16\pi G} f(T)\, d^4x \tag{71}$$

If general relativity is correct, we have to assume that the $f(T)$ function proposed has to revert back to T at early times, since we suspect a late time accelerating expansion. In **Chapter 2** we have also shown that in an isotropic, homogeneous FLRW universe $T = -6H^2$, and at early times $H = \frac{\dot{a}}{a} \gg 1$ since $a(t)$ will be very small. So we conclude that $f(T) \to T$ when $|T| \propto |H^2| \to \infty$, and the extra term that causes the acceleration should dominate when H is very small.

The next condition is that we want to make the $f(T)$ function easily related to the ΛCDM model at current times, because the ΛCDM model explains our observable universe reasonably well at present time. Thus we expect $f(T) \to T + 2\Lambda$ at $z = 0$, or at $H = H_0$ (where Λ is a constant). As there are 2 free parameters in the proposed $f(T)$functions, we should also expect that the function should revert to ΛCDM at a specific combination of parameters in order for easy comparison between models. Since it is arbitrary, it is decided to be set such that when $n = 0$, the $f(T)$ function should resemble the equation for cosmological constant.

So to summarize, the conditions to set the $f(T)$ functions are

1. $f(T) \to T$ when $T \to -\infty$
2. $f(T) \to T + 2\Lambda$ at $T = T_0$
3. $f(T) \to T + 2\Lambda$ when $n = 0$.

To ensure that these 3 constraints are easily satisfied, functions of the form of $f(T) = T + \alpha g(T, n)$ are proposed, where α is a constant, and $g(T, n)$ is a function of T and n respectively, and n will act as our free varying parameter. Now that the constraints of the proposed $f(T)$ functions are defined, we shall proceed to obtain a general solution for these $f(T)$ functions.

4.2.2 General Solution for $f(T) = T + \alpha g(T, n)$

Before we proceed to define our $H(z)$ function, we need to modify equation (44). We let ρ be

$$\rho = \rho_M + \rho_R \tag{72}$$

where ρ_M and ρ_R are the densities of matter and radiation of our universe. The expressions for ρ_M and ρ_R can be derived from the continuity equation (which is from the conservation of energy, $\nabla_\mu T^{\mu\nu} = 0$),

$$\frac{d}{da}(\rho a^3) + 3Pa^2 = 0 \quad \Rightarrow \quad \frac{1}{\rho}\frac{d\rho}{dt} + \frac{1}{a}\frac{da}{dt}3(1+w) = 0. \tag{73}$$

From **Chapter 2**, we learned that $w = 0$ for matter, and $w = \frac{1}{3}$ for radiation. So solving equation (73) for matter and radiation, we get

$$\rho_M = \rho_{m,0}\left(\frac{a_0}{a}\right)^3, \qquad \rho_R = \rho_{r,0}\left(\frac{a_0}{a}\right)^4. \tag{74}$$

Here the subscript 0 represents the value of that parameter at present time. Using equation (49), we substitute a with z:

$$\rho_M = \rho_{m,0}(1+z)^3, \qquad \rho_R = \rho_{r,0}(1+z)^4. \tag{75}$$

We further define Ω_M and Ω_R, the mass and radiation density parameters, where

$$\Omega_i = \frac{8\pi G}{3H^2c^2}\rho_i. \tag{76}$$

Plugging in equation (75) and (76), equation (44) becomes

$$12H^2 f'(T) + f(T) = 6H_0^2\left[\Omega_{m,0}(1+z)^3 + \Omega_{r,0}(1+z)^4\right]. \tag{77}$$

Now setting $f(T) = T + \alpha g(T,n)$ and $T = -6H^2$, we get

$$6H^2 + \alpha[12H^2 g'(T,n) + g(T,n)] = 6H_0^2\Omega(z). \tag{78}$$

Here the short hand notation $\Omega(z) = \Omega_{m,0}(1+z)^3 + \Omega_{r,0}(1+z)^4$, and therefore $\Omega(0) = \Omega_{m,0} + \Omega_{r,0}$. We can solve for α by using the fact that when $z = 0$, $H = H_0$. So α takes the form

$$\alpha = -\frac{6H_0^2[1-\Omega(0)]}{12H_0^2 g'(T_0,n) + g(T_0,n)}. \tag{79}$$

Equation (78) and (79) will be the starting point to turn all three of the following $f(T)$ functions into $H(z)$ equations that will be used to fit our observational constraints. Three $f(T)$ functions have been proposed here, and the terms $g(T,n)$ take the form of reciprocal power, exponential and hyperbolic tangent respectively. In all functions we have assumed an isotropic, homogeneous FLRW universe, and thus $T = -6H^2$.

4.2.3 $f(T)$ Function 1: Reciprocal Power

$$f_1(T) = T + \alpha\left(\frac{T_0}{T}\right)^n \tag{80}$$

Here a function with an additional term proportional to $\frac{1}{T^n}$, with $T_0 = -6H_0^2$ is suggested. This function resembles the function proposed by Bengochea and team,[14] but is formulated with different notation. It is used as a consistency check for the coding of χ^2 plots, so that the results can be compared. It can be easily shown that conditions 1 to 3 are satisfied by inducing the conditions in section **4.2.1**.

Now we abstract information from equation (80),

$$g(T,n) = \alpha\left(\frac{T_0}{T}\right)^n = \alpha\left(\frac{H_0^2}{H^2}\right)^n \tag{81}$$

$$g'(T,n) = \frac{n}{T_0}\left(\frac{T_0}{T}\right)^{n+1} = -\frac{n}{6H_0^2}\left(\frac{H_0^2}{H^2}\right)^{n+1}, \tag{82}$$

we fit equations (81) and (82) into equation (78), we get

$$6H^2 + \alpha\left(\frac{H_0^2}{H^2}\right)^n (2n+1) = 6H_0^2\Omega. \tag{83}$$

We proceed to get rid of α by using equation (79),

$$\alpha = -\frac{6H_0^2}{2n+1}\left(1 - \Omega_{m,0} - \Omega_{r,0}\right), \tag{84}$$

we then substitute α back to equation (81) to get

$$6H^2 + -6H_0^2\left(1 - \Omega_{m,0} - \Omega_{r,0}\right)\left(\frac{H_0^2}{H^2}\right)^n = 6H_0^2\Omega. \tag{85}$$

Finally, rearranging the terms, we get

$$\left(\frac{H}{H_0}\right)^{2n+2} - \left(\frac{H}{H_0}\right)^{2n}\Omega(z) - 1 + \Omega(0) = 0. \tag{86}$$

We have successfully derived our $H(z)$ function for $f_1(T)$. Here we note that an expression of $H(z)$ cannot be found explicitly, and thus root finding methods need to be

used to numerically find the value of H given values of $\Omega_{m,0}$ and n. It is also important to note that from equation (72), condition 1 will not be satisfied if $n < -1$, since $f(T) \to \infty$ as $T \to \infty$. Thus, this $f(T)$ model is only valid for $n \geq -1$. It is expected that the results of constraining this model should agree with Bengochea's results if the same tests were used.

4.2.4 $f(T)$ Function 2: Exponential

$$f_2(T) = T + \alpha e^{-n\frac{T}{T_0}} \tag{87}$$

Here we have a function with an additional term which gives a negative exponential. This equation was proposed as a modification to Linder's model, $f(T) = T + \alpha T\left(1 - e^{-p\frac{T}{T_0}}\right)$, which he got the motivation from his $f(R)$ model in a previous work.[38] Note that in Linder's model, his function does not revert to the ΛCDM model, and Linder did not conduct an observational constraint on his model. Doing our usual calculations just like section **4.2.3**,

$$g(T,n) = e^{-n\frac{T}{T_0}} = e^{-n\frac{H^2}{H_0^2}} \tag{88}$$

$$g'^{(T,n)} = -\frac{n\alpha}{T_0}e^{-n\frac{T}{T_0}} = \frac{n}{6H_0^2}e^{-n\frac{H^2}{H_0^2}} \tag{89}$$

$$\alpha = -\frac{6H_0^2[1-\Omega(0)]}{(2n+1)e^{-n}}. \tag{90}$$

With these information, equation (78) gives us

$$\left(\frac{H}{H_0}\right)^2 - \frac{2n\left(\frac{H}{H_0}\right)^2 + 1}{2n+1}e^{n\left[1-\left(\frac{H}{H_0}\right)^2\right]}[1-\Omega(0)] - \Omega(z) = 0. \tag{91}$$

Once again $H(z)$ cannot be found explicitly, and numerical methods are required to get the value of H. In this model, we see that there is a singularity when $n = -\frac{1}{2}$. Technically, this $f(T)$ model is only valid when $n \geq 0$, since a negative n value will not satisfy condition (1). As per usual, it can be easily proven that conditions 2 and 3 are satisfied.

4.2.5 $f(T)$ Function 3: Hyperbolic Tangent

$$f_3(T) = T + \alpha\left[1 - \tanh n\left(\frac{T}{T_0}\right)\right] \tag{92}$$

This function has an additional term of a hyperbolic tangent function. This function may look similar to Wu's model, $f(T) = T + \alpha(-T)^n \tanh\frac{T_0}{T}$, but Wu's model had a different motivation: he suggested a model that fits the phantom divide line crossing (the crossing of $w < -1$).[3] Once again the usual mathematics similar to the previous sections are done,

$$g(T, n) = 1 - \tanh n\left(\frac{T}{T_0}\right) = 1 - \tanh n\left(\frac{H^2}{H_0^2}\right) \tag{93}$$

$$g'^{(T,n)} = -\frac{n}{T_0}\operatorname{sech}^2 n\left(\frac{T}{T_0}\right) = \frac{n}{6H_0^2}\operatorname{sech}^2 n\left(\frac{H^2}{H_0^2}\right) \tag{94}$$

$$\alpha = -\frac{6H_0^2[1 - \Omega(0)]}{1 + 2n\operatorname{sech}^2 n - \tanh n}. \tag{95}$$

Substituting these slightly more complicated-looking equations into equation (78), we get

$$\left(\frac{H}{H_0}\right)^2 - \frac{1 + 2n\left(\frac{H}{H_0}\right)^2 \operatorname{sech}^2 n\left(\frac{H}{H_0}\right)^2 - \tanh n\left(\frac{H}{H_0}\right)^2}{1 + 2n\operatorname{sech}^2 n - \tanh n}[1 - \Omega(0)] - \Omega(z) = 0. \tag{96}$$

This model does not have a singularity, and due to the nature of the hyperbolic tangent function, it is valid at all n.

There are many other possible $f(T)$ functions that could be proposed, however due to the limitations of time, only 3 functions here could be tested. In the following section, the χ^2 tests for the 3 observational constraints used will be explained in detail.

4.3 χ^2 Tests

A χ^2 test is used to fit a particular equation to a set of data, and the smaller the value of the χ^2, the better the fit. Given a set of observed data O_i, the errors of the observed data σ_i, and a theoretical value $E(\vec{a}_i|\vec{\mu})$ for every O_i, where $\vec{a}_i = (a_{i1}, a_{i2}, \dots)$ are a set of parameters that both O_i and E depend on, and $\vec{\mu} = (\mu_1, \mu_2, \dots)$ are a set of free parameters that we can vary in the particular model, a χ^2 value can be represented by the following equation,

$$\chi^2(\vec{\mu}) = \sum_{data} \frac{[O_i - E(\vec{a}_i|\vec{\mu})]^2}{\sigma_i^2} \tag{97}$$

A χ^2 test minimizes the error in the least squares sense. Here we assume that there are only statistical errors and thus any systematic error terms have been neglected. In this project we have two free parameters from each model, they are n and $\Omega_{m,0}$, and the parameter that both the observed and theoretical value depend on is z. Thus our χ^2 equation can be written as

$$\chi^2(n, \Omega_{m,0}) = \sum_{data} \frac{\left[O_i - E(z_i|n, \Omega_{m,0})\right]^2}{\sigma_i^2} \tag{98}$$

The χ^2 statistics can be numerically obtained through some simple MATLAB programming. As there are two varying parameters, a two-dimensional grid of χ^2 statistics with n against $\Omega_{m,0}$ will be plotted, such that for every point $(n, \Omega_{m,0})$ on the graph, there would be a χ^2 value. The minimum χ^2 value will be obtained, and a contour plot on confidence intervals based on this value will be plotted. The three contour lines plotted will be of confidence intervals of 68.3%, 95.4% and 99.73% respectively, which are the 1σ, 2σ and 3σ lines. Since there are two varying parameters, these lines correspond to $(\chi^2_{min} + 2.3, \chi^2_{min} + 6.17, \chi^2_{min} + 11.8)$ respectively.[39] The χ^2 statistic formulas for each of the 3 distinct tests would be shown in the following sections.

4.3.1 SNE Test

We refer to equation (54) which gives us a theoretical value of μ_B, the distance modulus between the observers on earth and the supernova. Equation (98) now becomes

$$\chi^2(n, \Omega_{m,0}) = \sum_{580\ SNE} \frac{\left\{\mu_i - 5\log\left[100c(1+z_i)\int_0^{z_i} \frac{1}{H(\tilde{z})} d\tilde{z}\right]\right\}^2}{\sigma_i^2} \tag{99}$$

The Union2.1 data of 580 SNEs from the Supernova Cosmology Project will be used.

The equation for the SNE test may look pretty straightforward, but there is a minor problem here. As said earlier, there are only 2 free parameters that we are varying, being n and $\Omega_{m,0}$. However, a close look at the $H(z)$ equations showed that there are actually other parameters involved as well, namely H_0 and $\Omega_{r,0}$. Theoretically $\Omega_{r,0}$ should be negligibly small, since we currently have a matter dominated universe, fixing a small value of $\Omega_{r,0} = 5 \times 10^{-5}$ will solve the problem.[14] However, H_0 is not negligible, and is neither an important parameter needed to be determined explicitly.

The easiest way out is to set a particular value of H_0 (say, 68.5 km s^{-1} Mpc^{-1}), and continue with the fit. One could also fit a few values of H_0, and compare the different contour plots yielded (this method was conducted on $f_1(T)$ for the interest of the reader, see **Appendix B1**). However, there are better ways of solving the problem. In the following sections, two methods will be proposed: analytical marginalization and the minimized χ^2 method.

Analytical Marginalization

Marginalization of parameters is one way to get rid of free parameters that we do need by summing up the entire *likelihood* of that parameter in the function. The probability function of H_0 is proportion to χ^2 according to the formula[39]

$$P(H_0) \propto e^{-\frac{\chi^2}{2}}. \tag{100}$$

Since we do not know the exact value of H_0 and that we want it to be independent of the model, we can conduct an integration over all probabilities of H_0, so that the results include the likelihood of all possible H_0 values taken into account. We define χ_h^2 to be the analytically marginalized χ^2 value over the likelihood of h, where $H_0 = 100h$. We then have

$$\begin{aligned} e^{-\frac{\chi_h^2}{2}} &= \int_0^\infty e^{-\frac{\chi^2}{2}}\, dh \\ \chi_h^2 &= -2\ln \int_0^\infty e^{-\frac{\chi^2}{2}}\, dh. \end{aligned} \tag{101}$$

In order to simplify the integral, we first set $x(z) = \frac{H(z)}{H_0}$, and equation (54) gives

$$\begin{aligned} \mu_i &= 5\log\left[\frac{c(1+z_i)}{h}\int_0^{z_i}\frac{1}{x(\tilde{z})}\,d\tilde{z}\right] \\ &= 5\log\left[c(1+z_i)\int_0^{z_i}\frac{1}{x(\tilde{z})}\,d\tilde{z}\right] - 5\log h \\ \mu_i &= \mu_i^* - 5\log h. \end{aligned} \tag{102}$$

Plugging this relation back into equation (99), it now becomes

$$\chi_h^2 = -2\ln\int_0^\infty e^{-\frac{1}{2}\sum_{SNe}\frac{\{\mu_i-\mu_i^*+5\log h\}^2}{\sigma_i^2}}\,dh$$
$$= -2\ln\int_0^\infty e^{-\frac{1}{2}\sum\frac{(\mu_i-\mu_i^*)^2}{\sigma_i^2}-5\sum\frac{\mu_i-\mu_i^*}{\sigma_i^2}\log h-\frac{25}{2}\sum\frac{1}{\sigma_i^2}(\log h)^2}\,dh. \quad (103)$$

Using a change of variable $e^u = h,\ dh = e^u du,\ \log h = \frac{u}{\ln 10}$, we get

$$\chi_h^2 = -2\ln e^{-\frac{1}{2}\sum\frac{(\mu_i-\mu_i^*)^2}{\sigma_i^2}}\int_{-\infty}^\infty e^{-\frac{25}{2(\ln 10)^2}\sum\frac{1}{\sigma_i^2}u^2-2\left(\frac{5}{2\ln 10}\sum\frac{\mu_i-\mu_i^*}{\sigma_i^2}-\frac{1}{2}\right)u}\,du. \quad (104)$$

Finally, using the integral formula $\int_{-\infty}^{\infty} e^{-ax^2-2bx}dx = \sqrt{\frac{\pi}{a}}e^{\frac{b^2}{a}}$, we get its final form:

$$\chi_h^2 = \sum\frac{(\mu_i-\mu_i^*)^2}{\sigma_i^2} - \frac{\left(\sum\frac{\mu_i-\mu_i^*}{\sigma_i^2}-\frac{\ln 10}{5}\right)^2}{\sum\frac{1}{\sigma_i^2}} - \ln\left[\frac{2\pi(\ln 10)^2}{25\sum\frac{1}{\sigma_i^2}}\right]. \quad (105)$$

The term $\sum\frac{1}{\sigma_i^2}$ is independent of $\Omega_{m,0}$ and n, and therefore is treated as a constant. Equations (86), (91) and (96) have been conveniently expressed in the form of $\frac{H}{H_0}$ so that this calculation can be conducted easily. This is the χ^2 statistic marginalized over h.

Minimum χ^2

Another method to solve this problem is to use calculus to minimize the χ^2 with respect to h. We start from equation (99), plugging in equation (102), we get

$$\chi^2(n,\Omega_{m,0}) = \sum_{580\ SNE}\frac{\{\mu_i-\mu_i^*+5\log h\}^2}{\sigma_i^2}$$
$$\chi^2 = \sum\frac{(\mu_i-\mu_i^*)^2}{\sigma_i^2} + 10\sum\frac{\mu_i-\mu_i^*}{\sigma_i^2}\log h + 25\sum\frac{1}{\sigma_i^2}(\log h)^2 \quad (106)$$

Now to minimize χ^2, we let $\frac{d\chi^2}{d(\log h)} = 0$ (since minimizing with respect to h is the same as to $\log h$), so we get

$$\log h = -\frac{\sum\frac{\mu_i-\mu_i^*}{\sigma_i^2}}{5\sum\frac{1}{\sigma_i^2}}. \quad (107)$$

Substituting this result back to equation (106), we get

$$\chi^2 = \sum \frac{(\mu_i - \mu_i^*)^2}{\sigma_i^2} - \frac{\left(\sum \frac{\mu_i - \mu_i^*}{\sigma_i^2}\right)^2}{\sum \frac{1}{\sigma_i^2}}. \tag{108}$$

This is the minimized χ^2 statistic which is independent of H_0. This method yields an equation which differs from the one from the analytical marginalization method by 2 constants. It was tested that both these tests yield the same best fit values, but they differ by the value of χ^2 (this is verified in **Appendix B2**). This method was used by Bengochea, and will be the default method used for this SNE test. The MATLAB code for this test is shown in **Appendix A1**.

4.3.2 CMB/BAO Combined Test

The common method to conduct a CMB and a BAO test is to constrain them separately using $\mathcal{R}$ (equation (61)) and r_{BAO} (equation (64)),

$$\chi^2_{CMB} = \frac{\left[\mathcal{R}_i - \sqrt{\Omega_{m,0}} H_0 c \int_0^{z_{dec}} \frac{1}{H(\tilde{z})} d\tilde{z}\right]^2}{\sigma_i^2} \tag{109}$$

$$\chi^2_{BAO} = \sum_i^2 \frac{\left[r_{BAO,i} - \frac{r_s(z_d)}{D_V(z)}\right]^2}{\sigma_i^2} \tag{110}$$

where the observed values are $\mathcal{R} = 1.710 \pm 0.019$, $r_{BA0}(0.2) = 0.1905 \pm 0.0061$ and $r_{BAO}(0.35) = 0.1097 \pm 0.0036$. However, a more independent constraint can be achieved by combining these two tests into one. It is done by multiplying equations (59) and (64) to get a quantity A,

$$A = l_A r_{BAO} = \pi \frac{d_A^{(c)}(z_{dec})}{r_s(z_{dec})} \frac{r_s(z_d)}{D_V(z)} = \pi \frac{d_A^{(c)}(z_{dec})}{D_V(z)} \frac{r_s(z_d)}{r_s(z_{dec})}. \tag{111}$$

This quantity could be simplified by cancelling the dependence on the sound horizon scale. We implement the correction for the difference between the sound horizon at the end of the drag epoch and the sound horizon at last scattering by setting the ratio $\frac{r_s(z_d)}{r_s(z_{dec})} = 1.044 \pm 0.019$ (as calculated by Komatsu)[40]. Using the values of $\mathcal{R}$ and r_{BAO} above, we arrive at two observed quantities,

$$A_1 = \frac{d_A^{(c)}(z_{dec})}{D_V(0.2)} = 17.55 \pm 0.65, \tag{112}$$

$$A_2 = \frac{d_A^{(c)}(z_{dec})}{D_V(0.35)} = 10.10 \pm 0.38. \tag{113}$$

The theoretical value of A is

$$A_{th}(z) = \frac{d_A^{(c)}(z_{dec})}{D_V(z)} = \frac{\int_0^{z_{dec}} \frac{1}{x(\tilde{z})} d\tilde{z}}{\left[\frac{z}{x(z)}\left(\int_0^z \frac{d\tilde{z}}{x(\tilde{z})}\right)^2\right]^{\frac{1}{3}}} \tag{114}$$

where $x = \frac{H}{H_0}$, and the H_0 is cancelled out from the numerator and denominator. Thus our combined CMB/BAO χ^2 test would have the equation:

$$\chi^2_{C/B} = \sum_i^2 \frac{\left[A_i - A_{th}\left(z_i \middle| n, \Omega_{m,0}\right)\right]^2}{\sigma_i^2}. \tag{115}$$

The MATLAB code for this test can be found in **Appendix A2**.

4.3.3 OHD Test

The OHD χ^2 test is relatively simple. As the observed values of H_i and z_i have been measured by several groups, one only needs to calculate the values of $H(z)$ without any integration involved. In other words,

$$\chi^2_{OHD} = \sum_i^{15} \frac{\left[H_i - H\left(z_i \middle| n, \Omega_{m,0}\right)\right]^2}{\sigma_i^2}. \tag{116}$$

The data source of the 15 H_i values chosen to be used in this test (as used by Bengochea)[29] is summarized in the **Table 2**. The MATLAB code for this test can be found in **Appendix A3**.

With these 3 distinct χ^2 tests, we can find the total χ^2 value by simply adding them up, $\chi^2 = \chi^2_{SNE} + \chi^2_{C/B} + \chi^2_{OHD}$. The minimum χ^2 and best fit $\left(\Omega_{m,0}, n\right)$ values for each test will be recorded, contour plots will be plotted for every single tests, and the combined test results will also be analyzed and discussed.

z_i	H_i (km s^{-1} Mpc^{-1})	σ_i	Source
0.00	74.20	3.60	Riess et al.[41]
0.10	69.00	12.00	Stern et al.[31]
0.17	83.00	8.00	
0.27	77.00	14.00	
0.40	95.00	17.00	
0.48	97.00	62.00	
0.88	90.00	40.00	
0.90	117.00	23.00	
1.30	168.00	17.00	
1.43	177.00	18.00	
1.53	140.00	14.00	
1.75	202.00	40.00	
0.24	79.69	2.32	Gaztanaga et al.[42]
0.34	83.80	2.96	
0.43	86.45	3.27	

Table 2: Data used for the OHD Test

4.4 Root Finding: The Bisection Method

To conduct the SNE χ^2 test for $f_1(T)$, we need equations (86) and (108), rewritten as follows:

$$x^{2n+2} - x^{2n}\left[\Omega_{m,0}(1+z_i)^3 + \Omega_{r,0}(1+z_i)^4\right] - 1 + \Omega_{m,0} + \Omega_{r,0} = 0 \tag{117}$$

$$\chi^2 = \sum \frac{\left\{\mu_i - 5\log\left[c(1+z_i)\int_0^{z_i}\frac{1}{x(\tilde{z})}d\tilde{z}\right]\right\}^2}{\sigma_i^2} - \frac{\left\{\sum \frac{\mu_i - 5\log\left[c(1+z_i)\int_0^{z_i}\frac{1}{x(\tilde{z})}d\tilde{z}\right]}{\sigma_i^2}\right\}^2}{\sum\frac{1}{\sigma_i^2}}. \tag{118}$$

Since $x(z)$ is not explicitly defined, the integration cannot be done analytically. To solve the integration, we need to use root finding methods to obtain the value of x, and then use numerical integration methods to solve for the integral. Rewriting the $H(z)$ equation of $f_1(T)$ as

$$F(x) = x^{2n+2} - x^{2n}\left[\Omega_{m,0}(1+z_i)^3 + \Omega_{r,0}(1+z_i)^4\right] - 1 + \Omega_{m,0} + \Omega_{r,0} \tag{119}$$

Given values of z_i, $\Omega_{m,0}$, $\Omega_{r,0}$ and n, we can find x by letting $F(x) = 0$, and x would be the root of the equation. In order to do this numerically, the bisection method is used, and it works as follows.

Suppose the root of $F(x)$ is between the interval (a, b). We find values of $F(a)$, $F(b)$ and $F\left(\frac{a+b}{2}\right)$. The strategy is to halve the given interval, then select the subinterval where there is a sign change in $F(x)$ between the two ends. This process is repeated by improving the brackets, halving the intervals and retaining the interval containing the root, until the upper and lower limit approaches the root, $|b - a| \leq \varepsilon$ where ε is the desired precision required. Thus the root will have the precision of $\pm\varepsilon$, and it will be the output of the code. A simple bisection method MATLAB code will look like the following:

```
function root = bisection(f, left, right)
% f           = the function involved
% left/right = lower/upper boundary of the bracketed root
tolerance    = 1e-10;
error        = 1e8;
fLeft        = f(left);
fRight       = f(right);

while(error > tolerance)
    middle  = (left + right)/2;
    fMiddle = f(middle);
    if (fLeft*fMiddle <= 0)
        right  = middle;
        fRight = fMiddle;
    else
        left  = middle;
        fLeft = fMiddle;
    end

    error = abs(right - left);
    root  =  middle;
end
```

Fig. 3: MATLAB Code for the Bisection Method

In actual fact, there are many other root finding methods, like the Newton-Raphson method, Secant Method, Brent's Method and etc. The bisection method is said to be the slowest method, as the number of iterations taken to get the root is of the order $\frac{\ln\frac{|x_2-x_1|}{\varepsilon}}{\ln 2}$.[43] However, there are 2 reasons why the bisection method was chosen for this project. Firstly, although other methods have lesser steps to get to the root, the process requires differentiation, which in fact slows down the computer processing speed when the root finding method is repeated multiple times. The SNE test for example, requires the root finding code to repeat about 3600 times in order to get one single χ^2 value, and the bisection method turned out to be a faster solution. The second

reason is that while other methods suffer the possibility of deviations from the root bracket, the bisection method doesn't, and it is considered the safest method among all. Thus in all cases, the bisection method will be used to find the root of $x(z)$.

4.5 Numerical Integration: The Gauss-Legendre Quadrature

As it can be seen in equations (117) and (118), the integration cannot be done analytically, and thus we need to rely on numerical methods to get the integration done. There are many numerical integration methods available, like the trapezoidal rule, Romberg integration and Monte Carlo Integration,[43] but in this project, the Gauss-Legendre quadrature will be used.

Any integral can be approximated by a quadrature, with the form

$$\int_a^b f(x)\,dx = \sum_{m=1}^{N} W_m f(x_m) \tag{120}$$

where W_m are the weights, and x_m are the *abscissas* (the values of x where the integral is evaluated at). W_m and x_m are unknowns, and can be found by expecting $f(x)$ to be exact polynomials, such that $f(x) = 1, x, x^2, \dots, x^{2N-1}$. This method works something like the trapezoidal rule, except that instead of N panels of fixed widths, this method uses N weighted panels with different widths. This method works best within a limit of $[-1,1]$, so by changing the integration limits in equation (120), we get

$$\begin{aligned}\int_a^b f(x)\,dx &= \frac{b-a}{2}\int_{-1}^{1} f\left(\frac{b-a}{2}+\frac{b-a}{2}\xi\right)d\xi \\ &= \frac{b-a}{2}\sum_{i=1}^{n} W_i f\left(\frac{b-a}{2}+\frac{b-a}{2}\xi_i\right).\end{aligned} \tag{121}$$

We further set $n = 3$, and setting the integral range $[a, b] = [0, z]$ (which happens to be the integral range for all the integrations involved in this project), equation (121) now turns into

$$\int_0^z f(\tilde{z})\,d\tilde{z} = \frac{z}{2}\sum_{i=1}^{3} W_i f\left(\frac{z}{2}(1+\xi_i)\right). \tag{122}$$

The values $W_1, W_2, W_3, \xi_1, \xi_2$ and ξ_3 can be calculated using the Gram-Schmidt orthogonalization of functions, which results in the formation of Legendre

polynomials.[43] In simple terms, the values of ξ_i are the roots of the n-th Legendre polynomial $P_n(x)$, while the values of W_i are obtained using Gaussian integration of the Legendre polynomials. While the higher the value of n the more accurate the results, the side effect would be that the expression of the integration would have many terms, and thus an optimum $n = 3$ is used. The values of W_i and ξ_i are well known and can be obtained online.[44] For $n = 3$, we have

$$P_3(\xi) = \frac{1}{2}(5\xi^2 - 3)\xi, \tag{123}$$

$$\xi_1 = 0, \qquad \xi_2 = \sqrt{\frac{3}{5}}, \qquad \xi_3 = -\sqrt{\frac{3}{5}}, \tag{124}$$

$$W_1 = \frac{8}{9}, \qquad W_2 = W_3 = \frac{3}{9}. \tag{125}$$

So with these information, equation (122) now becomes

$$\int_0^z f(\tilde{z})\, d\tilde{z} = \frac{z}{2}\left[\frac{8}{9}f\left(\frac{z}{2}\right) + \frac{3}{9}f\left(\frac{z}{2}\left(1 + \sqrt{\frac{3}{5}}\right)\right) + \frac{3}{9}f\left(\frac{z}{2}\left(1 - \sqrt{\frac{3}{5}}\right)\right)\right]. \tag{126}$$

Therefore given a function $f(x)$, we can use Gauss-Legendre quadrature to solve the integration by working with $f(x)$ itself without any integration involved. The accuracy of the integration results can be further improved by dividing the integration into k equal parts,

$$\int_0^z f(\tilde{z})\, d\tilde{z} = \sum_{r=1}^{k} \frac{z}{2k}\left[\frac{8}{9}f\left(\frac{rz}{2k}\right) + \frac{3}{9}f\left(\frac{z}{2k}\left(r + \sqrt{\frac{3}{5}}\right)\right) + \frac{3}{9}f\left(\frac{z}{2k}\left(r - \sqrt{\frac{3}{5}}\right)\right)\right]. \tag{127}$$

The integration gets more and more accurate with higher values of k (the number of panels), but however, will slow down the integration process in MATLAB. Thus different optimum values of k will be assigned to each test depending on the integration limits. The MATLAB code for Gauss-Legendre integration is shown in **Fig. 4**.

With the necessary bisection and integration numerical methods, we can proceed to solve the χ^2 values for each distinct χ^2 test for the three different $f(T)$ functions, and plot their contour plots. The results of this project will be shown in the next chapter.

```
function integral = gauss_legendre_quadrature(f,a,b,n)
% a, b = limits of integration
% n    = the number of subintervals the integration is to be divided

h2   = (b-a)/(2*n);
sq35 = sqrt(0.6); % abscissa
w1   = 5/9;       % weights, x = +-sqrt(0.6)
w2   = 8/9;       % weights, x = 0
x    = linspace(a,b,n+1);
sum  = 0;

for (i = 1:n)
    sum = sum + w1*f(x(i) + h2 - sq35*h2);
    sum = sum + w2*f(x(i) + h2);
    sum = sum + w1*f(x(i) + h2 + sq35*h2);
end

integral = h2*sum;
```

Fig. 4: MATLAB Code for the Gauss-Legendre Quadrature

Chapter 5

RESULTS

In the following pages, the individual χ^2 contour plots of the SNE, CMB/BAO and OHD tests for each $f(T)$ function will be shown, and the best fit values of $\Omega_{m,0}$, n and their respective χ^2_{min} values will be tabulated. The χ^2 values obtained for each constraint test will be added together to get a total χ^2 value, and the overall best fit values from the combined SNE+CMB/BAO and SNE+CMB/BAO+OHD tests for the three $f(T)$ functions will be compared with one another and to the ΛCDM model.

5.1 Function 1: $f_1(T) = T + \frac{\alpha}{\left(T/T_0\right)^n}$

The 3 graphs in the following page shows the contour plots of the 2-dimensional χ^2 tests with n plotted against $\Omega_{m,0}$, and their respective confidence intervals at 68.3%, 95.4% and 99.73% respectively. The small black crosses indicate the point $(\Omega_{m,0}, n)$ which yields the χ^2_{min} respectively. Data from all three plots showed that the $f_1(T)$ model favors a non-zero n value (with the SNE test having a best fit very close to $n = 0$), although the ΛCDM model ($n = 0$) still lies within the 1σ region of the best fit. The CMB/BAO test yields a significantly higher value of n compared to the other two tests (comments in **Chapter 6**). The data obtained from the χ^2 tests are summarized in the following table:

χ^2 Test	$\Omega_{m,0}$	n	χ^2_{min}
SNE	$0.28^{+0.03}_{-0.03}$	$0.02^{+0.22}_{-0.19}$	562.2265
CMB/BAO	$0.28^{+0.03}_{-0.03}$	$4.77^{+n/a}_{-5.46}$	0.0574
OHD	$0.30^{+0.04}_{-0.04}$	$1.07^{+1.18}_{-0.63}$	8.1854

Table 3: Best Fit Values of $\Omega_{m,0}$ and n for $f_1(T)$ obtained from the 3 χ^2 Tests Conducted

Bengochea et al had also conducted a test with this same $f(T)$ model, and we find that his CMB/BAO test results gives $(\Omega_{m,0}, n) = \left(0.28^{+0.02}_{-0.02}, 4.58^{+n/a}_{-4.87}\right)$, in which the value of n is consistent within 4.1% percentage difference. Bengochea did conduct tests for SNE and OHD too, however the data he used for the SNE test was the older version (Union2), and he did not state explicitly his results of the OHD test. Thus it is not possible to compare these results obtained with the results of his work.

For $f_1(T)$, the SNE test was also done using analytical marginalization and the fixed H_0 method for values between 68 to 72 km s^{-1} Mpc^{-1}. The results of the analysis will be tabulated in **Appendix B1** and **B2**.

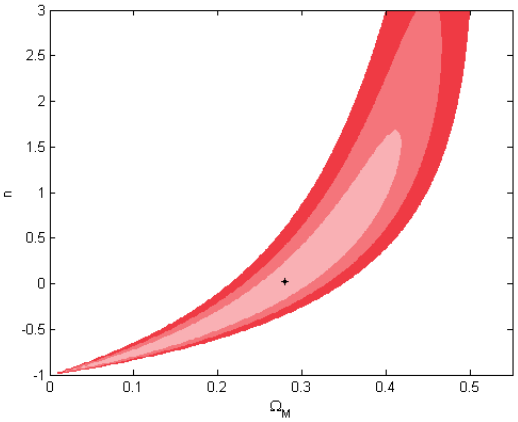

Fig. 5a: SNE Test for $f_1(T)$

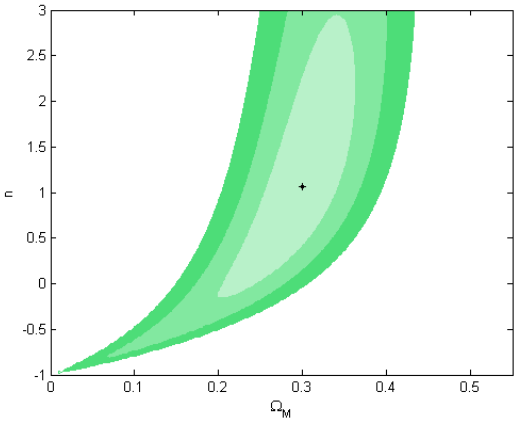

Fig. 5b: OHD Test for $f_1(T)$

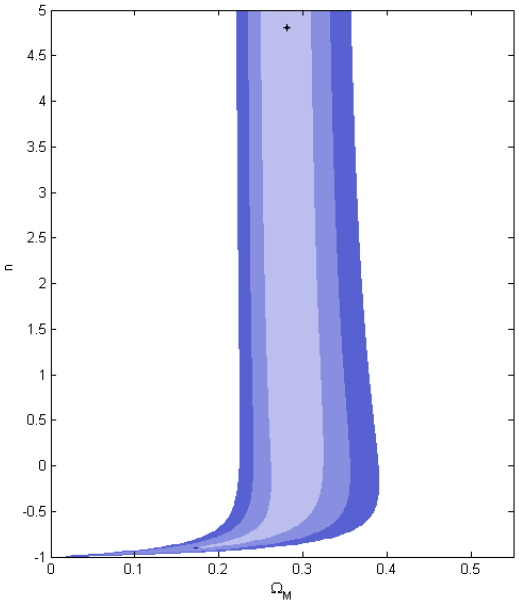

Fig. 5c: Combined CMB/BAO Test for $f_1(T)$

5.2 Function 2: $f_2(T) = T + \alpha e^{-n\frac{T}{T_0}}$

The 3 graphs in the following page shows the χ^2 contour plots of for $f_2(T)$. It can be seen that contour plot for the OHD test contains two minimum points, in which only one is the true minimum. The contour plot for the CMB/BAO test showed there is a drastic cut after $n < 0$, and this weird property will be discussed in **Chapter 6**. The results once again showed that a non-zero n is favored over the ΛCDM model, and the SNE test once again showed a best fit very close to $n = 0$. All the tests have the ΛCDM model included

in the 1σ region, but the CMB/BAO test has it at its borderline. The results of these individual tests are summarized in **Table 4**.

χ^2 Test	$\Omega_{m,0}$	n	χ^2_{min}
SNE	$0.29^{+0.04}_{-0.02}$	$-0.05^{+0.85}_{-0.05}$	562.2252
CMB/BAO	$0.28^{+0.03}_{-0.03}$	$5.57^{+n/a}_{-5.55}$	0.0463
OHD (upper)	$0.31^{+0.04}_{-0.04}$	$1.79^{+1.46}_{-0.72}$	8.3925
OHD (lower)	$0.22^{+0.03}_{-0.02}$	$0.01^{+0.26}_{-0.07}$	9.8785

Table 4: Best Fit Values of $\Omega_{m,0}$ and n for $f_2(T)$ obtained from the 3 χ^2 Tests Conducted

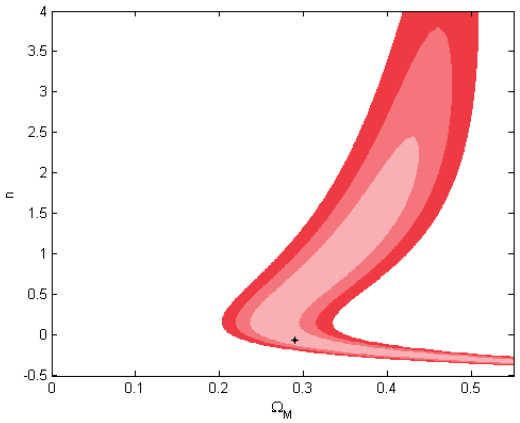

Fig. 6a: SNE Test for $f_2(T)$

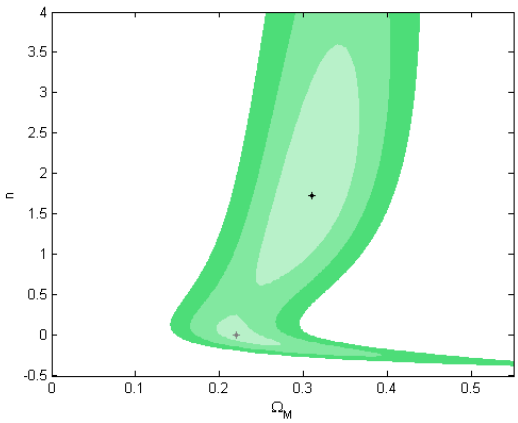

Fig. 6b: OHD Test for $f_2(T)$

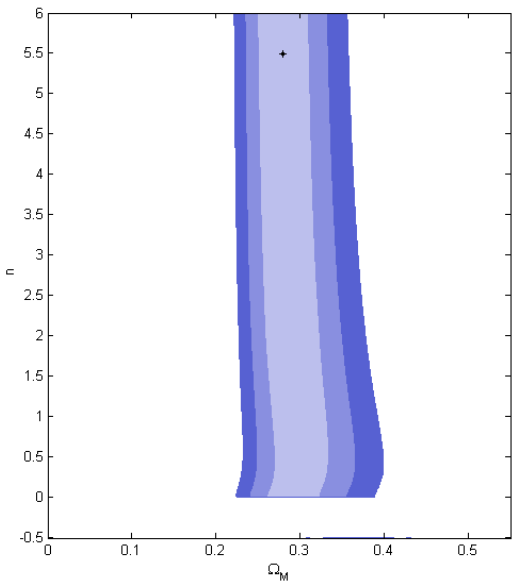

Fig. 6c: Combined CMB/BAO Test for $f_2(T)$

5.3 Function 3: $f_3(T) = T + \alpha\left[1 - \tanh n\left(\frac{T}{T_0}\right)\right]$

The 3 graphs below shows the χ^2contour plots for $f_3(T)$. The contours are seen to have twists between the region $-0.5 < n < 0.5$. In this plot, we see that the SNE test on $f_3(T)$ is shown to have greater deviation from the ΛCDM model compared to the previous 2 models. The OHD test showed that there are two minimum points, in which the absolute minimum point is at the lower region. This time, all three tests favored a non-zero value of n, but unlike previously, only the OHD test had the ΛCDM results outside of the 1σ region. The data obtained are summarized in **Table 5**.

χ^2 Test	$\Omega_{m,0}$	n	χ^2_{min}
SNE	$0.26^{+0.03}_{-0.02}$	$0.11^{+0.36}_{-0.14}$	562.2217
CMB/BAO	$0.28^{+0.03}_{-0.03}$	$2.79^{+n/a}_{-3.40}$	0.0461
OHD (lower)	$0.16^{+0.03}_{-0.04}$	$-0.52^{+0.13}_{-0.06}$	7.3965
OHD (upper)	$0.31^{+0.03}_{-0.03}$	$1.06^{+0.46}_{-0.22}$	8.4235

Table 5: Best Fit Values of $\Omega_{m,0}$ and n for $f_3(T)$ obtained from the 3 χ^2 Tests Conducted

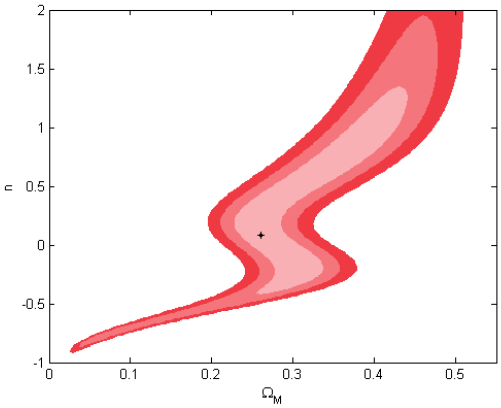

Fig. 7a: SNE Test for $f_3(T)$

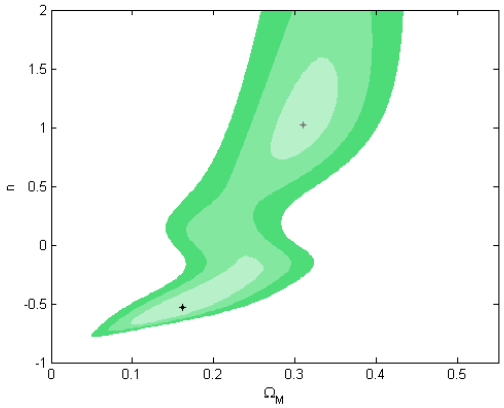

Fig. 7b: OHD Test for $f_3(T)$

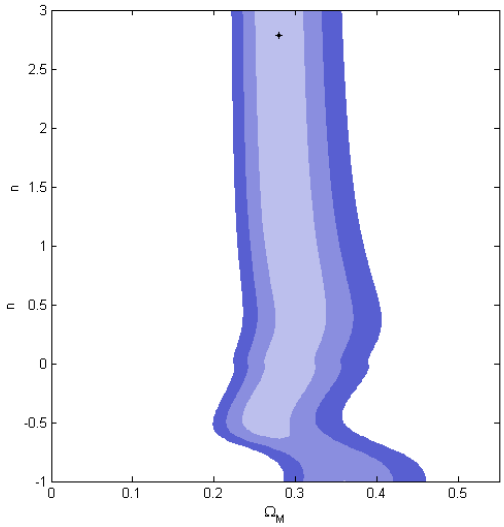

Fig. 7c: Combined CMB/BAO Test for $f_3(T)$

5.4 Combination and Comparison of Results

We have seen the individual results of $f_1(T)$, $f_2(T)$ and $f_3(T)$. As not all constraints by themselves are strong, we need to combine the results by adding the χ^2 values. The most reliable combination would be the SNE + CMB/BAO results, while the SNE + CMB/BAO + OHD results will be tabulated for comparison. The combined results will be summarized in **Table 6** below:

$f(T)$	SNE + CMB/BAO			SNE + CMB/BAO + OHD		
	$\Omega_{m,0}$	n	χ^2_{min}	$\Omega_{m,0}$	n	χ^2_{min}
$f_1(T)$	$0.29^{+0.02}_{-0.02}$	$0.09^{+0.24}_{-0.20}$	562.8908	$0.29^{+0.02}_{-0.02}$	$0.26^{+0.23}_{-0.20}$	575.3784
$f_2(T)$	$0.30^{+0.02}_{-0.02}$	$0.58^{+0.34}_{-0.28}$	563.0011	$0.30^{+0.02}_{-0.02}$	$0.79^{+0.32}_{-0.22}$	576.1400
$f_3(T)$	$0.29^{+0.03}_{-0.02}$	$-0.07^{+0.19}_{-0.26}$	562.8907	$0.28^{+0.02}_{-0.02}$	$-0.12^{+0.14}_{-0.15}$	575.7724
ΛCDM	0.28	0.00	563.1666	0.27	0.00	577.1172

Table 6: Combined Best Fit Values of $\Omega_{m,0}$ and n for All Functions

The χ^2 contour plots for the SNE + CMB/BAO and SNE + CMB/BAO + OHD tests are shown in **Figs. 8** and **9**. As it can be seen, the combined tests for $f_2(T)$ results in a sharp lower end, and this is due to the sharp cut seen in the CMB/BAO test. As for $f_3(T)$, it has two minimum points for both combinations. The other minimum point for SNE + CMB/BAO + OHD plot is (0.31,0.64) with $\chi^2 = 577.1154$, while the one for SNE + CMB/BAO is (0.30,0.49) with $\chi^2 = 563.3699$.

From the results in **Table 5**, we can deduce that $f_2(T)$ the exponential function does not seemed to fit the data as good as $f_1(T)$ and $f_3(T)$, since it has a much higher χ^2_{min} value than the rest. The SNE + CMB/BAO tests for $f_1(T)$ and $f_3(T)$ yield results which are very close to ΛCDM model, and we can conclude that the ΛCDM model is still a very good approximation of our universe at the moment. The SNE + CMB/BAO + OHD test seemed to suggest that $f_1(T)$ is the best fit model. It also showed a deviated value of n from the ΛCDM model, which leads to the suggestion that if the OHD observational test is reliable, there might be small perturbations from the ΛCDM model, where the Lagrangian T might have additional corrected terms. This conclusion is supported by the fact that the best fit model using the SNE + CMB/BAO + OHD test is $f_1(T)$, and that the ΛCDM model is not within its 1σ region.

The different conclusion drawn from the two different combinations suggest that there are some discrepancies between the SNE and OHD test, and this will be discussed in the next chapter. Despite the differences in both different combinations, one result is certain: the analysis of the three functions consistently suggested $\Omega_{m,0} \approx 0.29$, which

means that the acceleration of our universe is caused by an approximate 29:71 ratio of matter and dark torsion fluid.

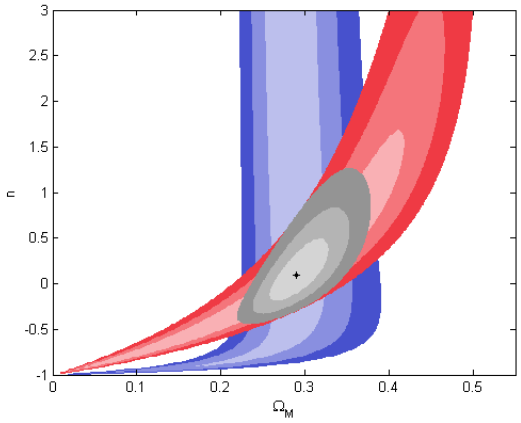

Fig. 8a: SNE + CMB/BAO Test for $f_1(T)$

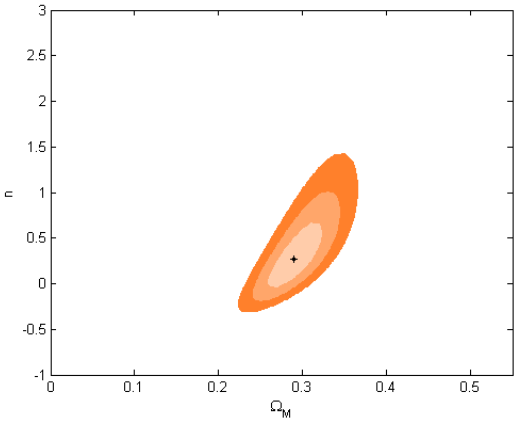

Fig. 9a: SNE + CMB/BAO + OHD Test for $f_1(T)$

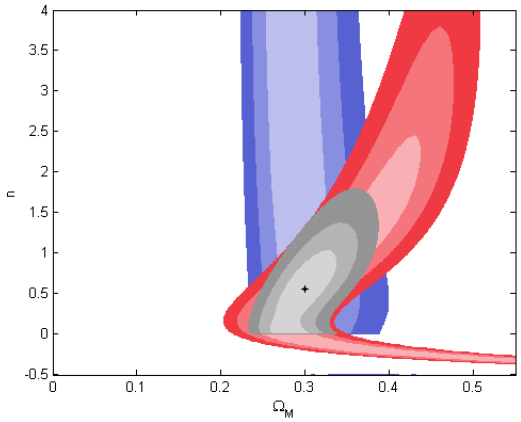

Fig. 8b: SNE + CMB/BAO Test for $f_2(T)$

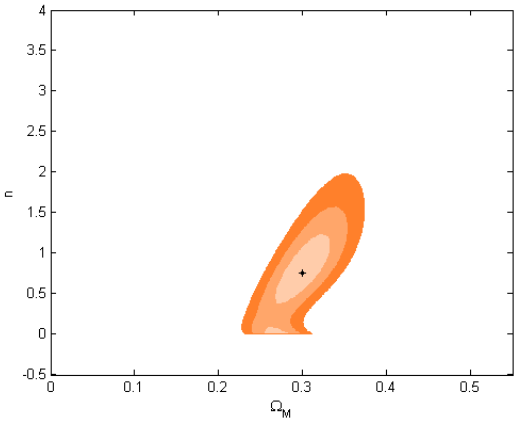

Fig. 9b: SNE + CMB/BAO + OHD Test for $f_2(T)$

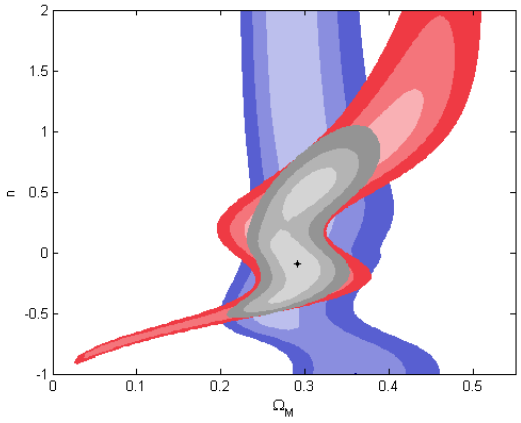

Fig. 8c: SNE + CMB/BAO Test for $f_3(T)$

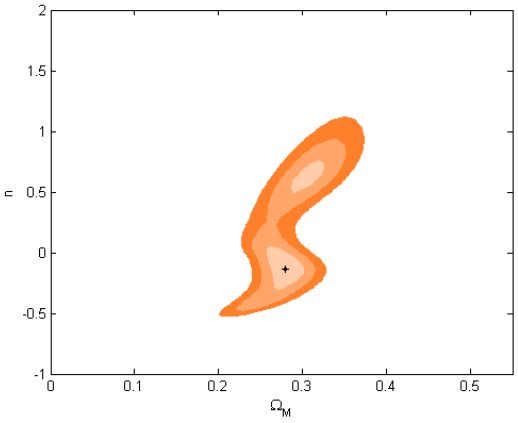

Fig. 9c: SNE + CMB/BAO + OHD Test for $f_3(T)$

Chapter 6

DISCUSSION AND SOURCES OF ERROR

6.1 Comments on the CMB/BAO Test

As it was shown in **Chapter 5**, the CMB/BAO test seemed to yield a much higher value of n compared to the other two tests for all $f(T)$ models. This is because the CMB and BAO tests are weak observational constraints on cosmological models (mentioned in **Chapter 3**), and the results lead us to suggest that its dependence on n is weak too. In other words, the value of n resulting from the CMB/BAO test should not be taken literally, but instead constrained together with other tests.

For $f_2(T)$, we see that there is a drastic cut in the graph of the CMB/BAO χ^2 test at the line $n = 0$ (**Fig. 6c**). After careful analysis, it was found that this is due to the exponential function in equation (91) and the top integral in equation (114), as shown below:

$$x^2 - \frac{2nx^2 + 1}{2n + 1} e^{n(1-x^2)}\left(1 - \Omega_{m,0} - \Omega_{m,0}\right) - \Omega(z) = 0 \qquad (128)$$

$$\int_0^{1090} \frac{1}{x(\tilde{z})} d\tilde{z} \qquad (129)$$

As the integration of the commoving angular diameter involves an integration of a significantly large z ($z = 1090$), the sudden jump in the root of equation (128) would be very large as n moves from 0 to -0.01, and thus the numerator in equation (114) will undergo a significant change. A simple plot of equation (128) in **Fig. 10** will visualize the problem.

Both plots in **Fig. 10** are plotted at fixed values of $\Omega_{m,0} = 0.28$ and $z = 1090$. As it is shown, the exponential value changes drastically when n passes from positive to negative, making the root for the equation changes drastically from 20843 to 41. This drastic change is only for the case when z is large, as it is tested that at $z = 0.35$, the root only changes from 1.167 to 1.168. Thus, the integration over such a large change during the transition from $n = 0$ to $n = -0.01$ has caused a sudden hike in the χ^2 value, and thus the drastic cut in the section. The fact that such a drastic cut exists in this model also leads us to suggest that such a model might not be a stable $f(T)$ model, as it is counter-intuitive to expect a cosmological model to behave in such a manner. The

higher χ^2_{min} value of $f_2(T)$ has also supported the argument that there are indeed better models than this that fits the universe.

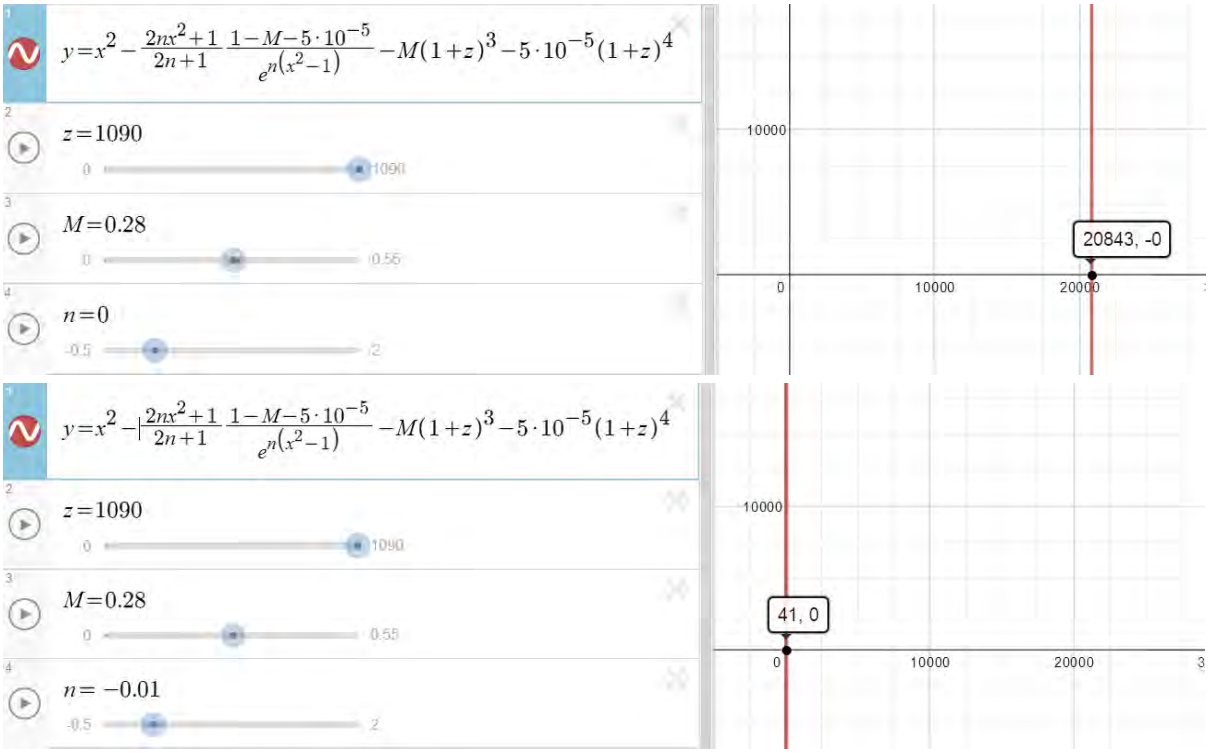

Fig. 10a & b: The plot of $x(z)$ for $f_2(T)$ at $\Omega_{m,0} = 0.28, z = 1090$ and $n = 0$ (top) and $n = -0.01$ (bottom) respectively.

6.2 Comments on $f_1(T)$ and $f_3(T)$

As it was shown in section 5, the best fit χ^2 values of $f_1(T)$ and $f_3(T)$ are very close to one another, although the two functions and their best fit values of n differ from one another. In order to determine which model is a better one, we have to take into account the physical picture of the model itself. There are a few arguments here to suggest that $f_1(T)$ would be a more viable model than $f_3(T)$.

If we see $f(T)$ models as small perturbation of the ΛCDM model, it is easier to believe that the small perturbation should be in the form of a reciprocal power than a hyperbolic tangent function. Besides, the shape of the contours of $f_3(T)$, and having 2 local minimum χ^2 values also lead us to suggest that there might be stability issues in $f_3(T)$. Thus it would be more intuitive to think that $f_1(T)$ is a better model than $f_3(T)$. However, these arguments are overshadowed by the fact that the values of n yield from the SNE + CMB/BAO tests are close to 0, in which a better conclusion, would still be that these models are indistinguishable with the ΛCDM model. It would be safer to conclude that a particular $f(T)$ model is better than the ΛCDM model if it has a much lower χ^2

value, and that it has a tighter constraint which rules out $n = 0$ from its confidence interval.

6.3 The Tension between SNE and OHD Test

Careful analysis on the SNE and OHD χ^2 contours had yield unexpected results. It is found that the 1σ region of the best fit values of $(\Omega_{m,0}, n)$ for the SNE and OHD tests do not coincide with one another. **Fig. 11a, b & c** below shows the 1σ region of the best fit values for the SNE (red) and OHD (green) tests:

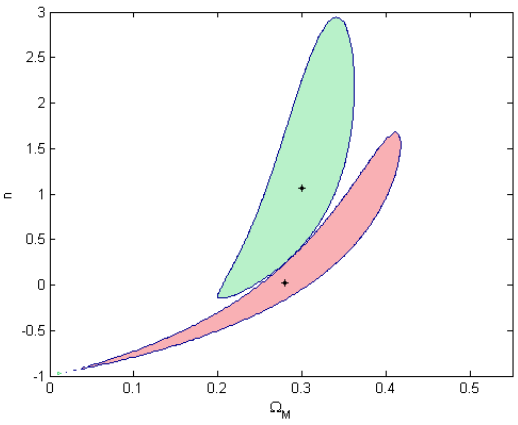

Fig. 11a: 1σ Contour of SNE & OHD Test for $f_1(T)$

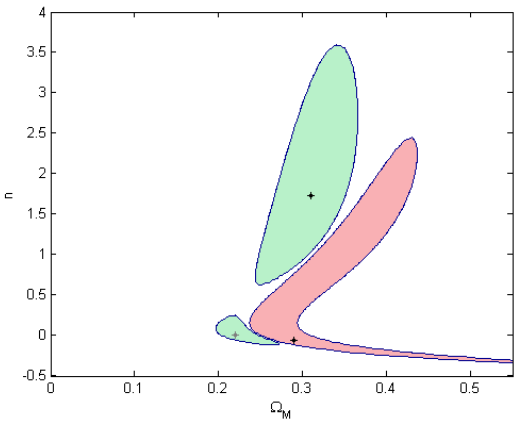

Fig. 11b: 1σ Contour of SNE & OHD Test for $f_2(T)$

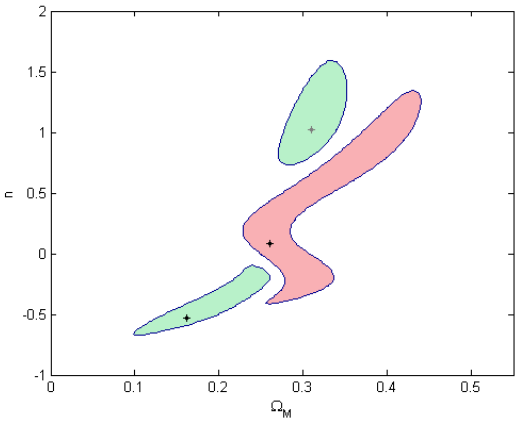

Fig. 11c: 1σ Contour of SNE & OHD Test for $f_3(T)$

The fact that both tests do not coincide is indeed puzzling. Not only that, it looked as if the contours were trying to 'avoid each other'. This is counter intuitive, since we expect observational constraints to be consistent with one another, and should have common confidence regions for us to gauge the best fit values. At the moment, it was found that no literature published had discussed on this results: most literature only mentioned that the values of $\Omega_{m,0}$ yield very similar results to that of the ΛCDM model.[30, 31]

There are a few possible explanations for this result. Firstly, the OHD test, by its very own nature, might be the problem itself. As the OHD test highly depends on the correct determination of the age of the galaxies, and the statistical differences of the redshifts, we expect calculation errors to be involved. Besides, in our case we only used 15 observed Hubble data, and we could increase the amount of our data to include more $H - z$ values to dilute the errors, like that of Farooq and Ratra, who used 28 data in their analysis.[45] Thus, due to the propagation of errors involved, the OHD test might not be a good stand-alone test at the moment. Another possible explanation is that the OHD test might be not sensitive to n, like the case of the CMB/BAO test. We notice that the error in n for the OHD test is larger than the SNE test. However, the best fit values are consistent at a certain value of $\Omega_{m,0}$, with the exception of $f_3(T)$. This problem can be solved by increasing the number of datasets and diluting the error, as mentioned earlier.

To verify whether such behavior occurs in other situations, the SNE and OHD test for dark energy was conducted (a plot of $\Omega_{m,0}$ against w, following the work of my UROPS[26]), and the same behavior was found for both tests (**Fig. 12c**).

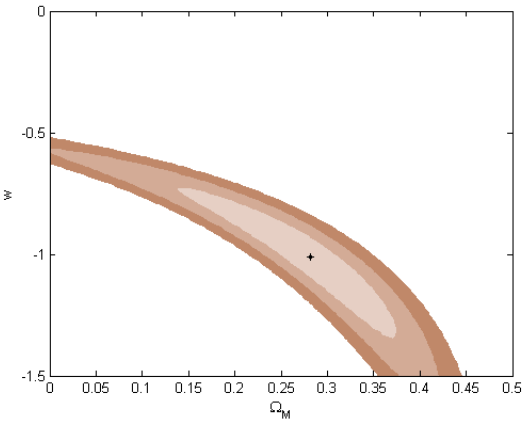

Fig. 12a: SNE Test for Dark Energy

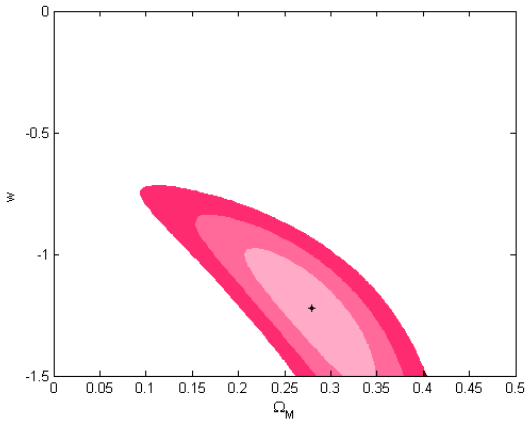

Fig. 12b: OHD Test for Dark Energy

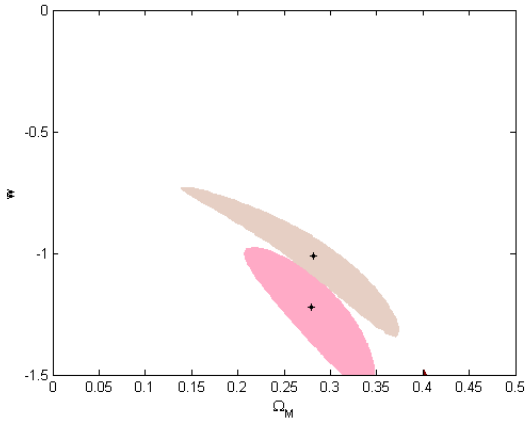

Fig. 12c: 1σ Region for SNE & OHD Tests for Dark Energy

Once again, they yield the same value of $\Omega_{m,0}$ of 0.28, but different values of n. The SNE test showed that source of cosmic acceleration is close to dark energy ($w = -1.01$), while the OHD test favored phantom energy ($w = -1.22$).

The explanations given above are not solid. In order to further investigate the problem, one needs to further understand how the SNE and OHD data were taken and measured. The in-depth analysis of the SNE and OHD tests could be a beneficial future project, it will test the viability and validity of both tests, and will help to constrain models better in the future.

6.4 Determination of the Value of H_0

Following the minimized χ^2 method used in the SNE test, it is found that we would be able to determine the favored value of H_0 for each $f(T)$ model through minor tweaking of equation (107). Rewriting it, we get

$$H_0 = 10^{2-\frac{\sum\frac{\mu_i-\mu_i^*}{\sigma_i^2}}{5\sum\frac{1}{\sigma_i^2}}} \text{ km s}^{-1} \text{ Mpc}^{-1}. \quad (130)$$

Plugging in the given the best fit values of n and $\Omega_{m,0}$, we will be able to find the best fit value of H_0 to the three models. The best fit values of H_0 obtained are quite consistent, they are 69.993, 70.002 and 69.989 km s^{-1} Mpc^{-1} respectively. Rounding off to 70km s^{-1} Mpc^{-1} , this results is equal to the results obtained by Reiss (74.2km s^{-1} Mpc^{-1}) within 5.6% percentage difference.

Although we have assumed that the SNE is test is the most reliable observational constraint of all, the determination of H_0 requires many other factors to be taken into account, thus this analysis only suggests the best fit values of H_0 for that particular model only, and cannot be generalized. Equation (130) merely acts as a quicker alternative for the user compared to plotting a 3-parameter ($\Omega_{m,0}, n, H_0$) fit on the models.

6.5 Recent Related Work

As mentioned earlier in this thesis, various other research groups have proposed many other $f(T)$ functions and used various observational constraints to fit their cosmological models. The functions $f_2(T)$ and $f_3(T)$ proposed here are the author's original work, while $f_1(T)$ is similar to Bengochea's proposed function.[14] The search for

a better $f(T)$ model with various motivations continues, and a summary list of various $f(T)$ functions proposed by various research groups is tabulated in **Appendix C** for the reference of the reader. Other recent research work on $f(T)$ gravity include the constraint on $f(T)$ models using cosmography[46], the study on cosmological perturbations[2], time-propagation and evolution of $f(T)$ gravity[19] and etc. There are also research groups which collect $f(T)$ functions from various authors to compare and fit with the latest data, like the work of Cardone[47] and Nesseris.[48]

6.6 Sources of Error

Throughout this project, the main sources of error would be the numerical methods of root finding and integrations. As the integration involves a reciprocal function, the numerical errors will be brought forward from the root finding part into the integral. One way to solve this problem would be to increase the accuracy of the bisection and the integration by decreasing the tolerance value of the bisection, and increasing the panels of integration involved. However, the more accurate the calculations, the more time it takes for calculations to complete, and thus optimum values of tolerance and integration panels have been set and chosen for each test to ensure a balance in time management and accuracy of data collected. Other sources of error would include human error in deriving equations, errors in copying data and errors in coding. All these errors could be reduced by conducting counter checks and consistency checks.

Chapter 7

CONCLUSION AND FUTURE WORK

7.1 Conclusion

From the SNE + CMB/BAO tests, we conclude that the $f(T)$ models tested are shown to be indistinguishable from the ΛCDM model, and that the ΛCDM model is still a reasonable best fit model to describe our universe (Nesseris made a similar conclusion too[48]). From the SNE + CMB/BAO + OHD tests, we conclude that there might be a certain positive perturbation from the ΛCDM model caused by dark torsion, and that $f_1(T)$, the reciprocal power model is the best fit model of our universe. In both cases, it is found that the mass density parameter $\Omega_{m,0} = 29 \pm 1\%$. Thus we conclude that, $f(T)$ gravity models are relatively good alternatives to dark energy, but the results are highly dependent on the observational constraints used.

7.2 Future Work

As much as how this project has achieved its goal to analyze different $f(T)$ gravity models and conclude its viability, there are still many areas where this work can be continued on. One could continue to use other different $f(T)$ functions to see whether they produce results similar to what was shown in this work. Since in this work MATLAB codes for χ^2 tests have been setup, it is very easy to continue the analysis by substituting other $f(T)$ functions. **Fig. 12** below shows just a few other examples of $f(T)$ functions that could be tried out.

$$f(T) = T + \alpha \operatorname{sech} n\left(\frac{T}{T_0}\right) \qquad f(T) = T + \alpha \operatorname{csch} n\left(\frac{T}{T_0}\right)$$

$$f(T) = T + \alpha \left[\coth n\left(\frac{T}{T_0}\right) - 1\right] \qquad f(T) = T + \alpha \left[\frac{\pi}{2} - \tan^{-1} n\left(\frac{T}{T_0}\right)\right]$$

$$f(T) = T + \alpha \cot^{-1} n\left(\frac{T}{T_0}\right) \qquad f(T) = T + \alpha \operatorname{csch}^{-1} n\left(\frac{T}{T_0}\right)$$

$$f(T) = T + \frac{\alpha}{\left[\ln\left(\frac{T}{T_0} + 1\right)\right]^n}$$

Fig. 13: Other Possible $f(T)$ Functions to be Tested

Other than that, further work could be done to improve the observational constraints on cosmological models. One could study their advantages and disadvantages, include other extra observational constraints, and further analyze which

observational tests are the most stable, suitable and reliable for cosmological model fittings. This is a very important aspect, since many new cosmological models and ideas are constantly produced, and it is of utmost importance for physicists to be fitting them with the best data and constraints available. An example from this work would be to study the OHD and SNE test critically, to understand why their best fit plots do not overlap within 1σ. Of course, as time goes by, the observational constraint would improve as the dataset expands, and thus a future work in the form of testing old cosmological models with new data is considered new work as well.

Lastly, it would also be important to study the theory itself, to study the detailed physics behind teleparallel gravity and $f(T)$ gravity. Although $f(T)$ gravity models are empirically defined, it is crucial that these models make sense: we want to know why the universe behaves with a perturbation of a reciprocal power function, and what is its physical meaning. It would be beneficial to understand the stability, time evolution of $f(T)$ gravity models, and most important of all, to ensure its consistency with the rest of the known physics theories available.

At the moment, humans are still far from fully understanding the vast universe that we live in. Researches in these areas are always limited by the precision of instrumentation and travelling speed. But as long as physicists continue to put in their effort in this research area, I believe that we will be closer and closer to fully understanding this mysterious universe that we live in.

APPENDIX A: MATLAB CODES

A1 SNE χ^2 Test MATLAB Code

```
function torsion_sne()
global mm nn z muB sigma2 c Omega_r
M           = dlmread('union21data.m');
z           = M(:,1);
muB         = M(:,2);
sigma2      = M(:,3).^2;
c           = 299792458;
Omega_r     = 5e-5;
chi2min     = 1e9;
Omega_m_min = 10;
n_min       = 10;

Omega_m = 0:0.01:0.55;
n       = -1:0.01:3;

Chi2     = ones(length(n),length(Omega_m));
sumerror = 0;

% value of the constant term
for (k = 1:length(sigma2))
    sumerror = sumerror + 1./sigma2(k);
end

% loop for the chi^2 matrix
for (I = 1:length(Omega_m))
    mm = Omega_m(i);

    for (j = 1:length(n))
        nn    = n(j);
        chistar = 0;
        64print64 = 0;

        for (l = 1:length(M))
            int     = gauss_legendre_quadrature(@inverseY,0,z(l),6);
            chistar = chistar + (5*log10((1 + z(l)).*int) -
                      muB(l)).^2./sigma2(l);
            64  print  64   =   64  print  64   +   (5*log10((1+z(l)).*int)-
muB(l))./sigma2(l);
        end
```

```
        chi2      = chistar - (65print65)^2/sumerror;
        Chi2(j,i) = chi2;
        disp(65print('(%g,%g)',Omega_m(i),n(j)));

        % Finding the minimum chi^2 value in the process of the loop.

        If (chi2min > chi2)
            chi2min     = chi2;
            Omega_m_min = Omega_m(i);
            n_min       = n(j);
        end
    end
end

% save the results into a file
dlmwrite('Chi2sne.m',Chi2,'precision','%.7f');

% display the results
disp(65print('(Omega_M,n) = (%g,%g)',Omega_m_min, n_min));

% plot the contour lines.
V = [chi2min+2.3, chi2min+6.17, chi2min+11.8];
contour(Omega_m, n, Chi2, v);
xlabel('Ω_M');
ylabel('n');


% the H(z) equation of the f(T) model
function l = f(x)
global nn mm zz Omega_r
l = x^2 - (2*nn*x^2 + 1)/(2*nn + 1)*(1 - mm - Omega_r)/exp(nn*(x^2 - 1)) -
    mm*(1 + zz)^3 - Omega_r*(1 + zz)^4;

function k = inverseY(z)
global zz
zz = z;
root = bisection(@f,0,5);
k = 1./root;
```

Fig. 14: MATLAB Code for the SNE χ^2 Test

A2 Combined CMB/BAO χ^2 Test MATLAB Code

```
function torsion_cmbbao()
global mm nn Omega_r
Omega_r     = 5e-5;
chi2min     = 1e9;
Omega_m_min = 10;
n_min       = 10;
zstar       = 1090;
z1          = 0.2;
z2          = 0.35;
Chi2        = ones(length(n),length(Omega_m));

Omega_m = 0:0.01:0.55;
n       = -1:0.01:3;

% loop for the chi^2 matrix
for (i = 1:length(Omega_m))
    mm = Omega_m(i);

    for (j = 1:length(n))
        nn   = n(j);
        d_A  = gauss_legendre_quadrature(@inverseY,0,zstar,2984);
        D_v1 = (z1*inverseY(z1)*(gauss_legendre_quadrature(@inverseY,0,z1,
               13))^2)^(1/3);
        D_v2 = (z2*inverseY(z2)*(gauss_legendre_quadrature(@inverseY,0,z2,
               13))^2)^(1/3);
        chi2 = (d_A/D_v1-17.55)^2/0.65^2 + (d_A/D_v2-10.10)^2/0.38^2;

        Chi2(j,i) = chi2;

        disp(sprintf('(%g,%g)',Omega_m(i),n(j)));

        % Finding the minimum chi^2 value in the process of the loop.
        if (chi2min > chi2)
            chi2min     = chi2;
            Omega_m_min = Omega_m(i);
            n_min       = n(j);
        end
    end
end

% save the results into a file
dlmwrite('Chi2cmbbao.m',Chi2,'precision','%.7f');

% display the results
```

```
disp(sprintf('(Omega_M,n) = (%g,%g)',Omega_m_min, n_min));

% plot the contour lines.
v = [chi2min+2.3, chi2min+6.17, chi2min+11.8];
contour(Omega_m, n, Chi2, v);
xlabel('\Omega_M');
ylabel('n');


% the H(z) equation of the f(T) model
function l = f(x)
global nn mm zz Omega_r
l = x^2 - (2*nn*x^2 + 1)/(2*nn + 1)*(1 - mm - Omega_r)/exp(nn*(x^2 - 1)) -
    mm*(1 + zz)^3 - Omega_r*(1 + zz)^4;

function k = inverseY(z)
global zz
zz = z;
root = bisection(@f,0.001,50000);
k = 1./root;
```

Fig. 15: MATLAB Code for the Combined CMB/BAO χ^2 Test

A3 OHD χ^2 Test MATLAB Code

```
function torsion_ohd()
global mm nn Omega_r H0
Omega_r     = 5e-5;
H0          = 74.2;
chi2min     = 1e9;
Omega_m_min = 10;
Chi2        = ones(length(n),length(Omega_m));

Omega_m = 0:0.01:0.55;
n       = -1:0.01:3;

Hdata = [74.2 69 83 77 95 97 90 117 168 177 140 202 79.69 83.8 86.45]';
sigma = [3.6 12 8 14 17 62 40 23 17 18 14 40 2.32 2.96 3.27]';
z     = [0 0.1 0.17 0.27 0.4 0.48 0.88 0.9 1.3 1.43 1.53 1.75 0.24 0.34
        0.43]';

% loop for the chi^2 matrix
for (i = 1:length(Omega_m))
    mm = Omega_m(i);

    for (j = 1:length(n))
        nn   = n(j);
        chi2 = 0;

        for (k = 1:length(z))
        chi2 = chi2 + (H(z(k)) - Hdata(k))^2/sigma(k)^2;
        end

        Chi2(j,i) = chi2;

        disp(sprintf('(%g,%g)',Omega_m(i),n(j)));

        % Finding the minimum chi^2 value in the process of the loop.
        if (chi2min > chi2)
            chi2min     = chi2;
            Omega_m_min = Omega_m(i);
            n_min       = n(j);
        end
    end
end

% save the results into a file
dlmwrite('Chi2ohd.m',Chi2,'precision','%.7f');
```

```
% display the results
disp(sprintf('(Omega_M,n) = (%g,%g)',Omega_m_min, n_min));

% plot the contour lines.
v = [chi2min+2.3, chi2min+6.17, chi2min+11.8];
contour(Omega_m, n, Chi2, v);
xlabel('\Omega_M');
ylabel('n');


% the H(z) equation of the f(T) model
function l = f(H)
global nn mm zz Omega_r H0
x = H/H0;
l = x^2 - (2*nn*x^2 + 1)/(2*nn + 1)*(1 - mm - Omega_r)/exp(nn*(x^2 - 1)) -
    mm*(1 + zz)^3 - Omega_r*(1 + zz)^4;

function root = H(z)
global zz
zz   = z;
root = bisection(@f,0.1,340);
```

Fig. 16: MATLAB Code for the OHD χ^2 Test

APPENDIX B: OTHER RESULTS

B1 Results for SNE Test with Fixed H_0 on $f_1(T)$

The SNE Test fixed H_0 test for $f_1(T)$ was done for $68 \leq H_0 \leq 72$, using the Union1.0, which was the first published data from the Supernova Cosmology Project, a compilation of only 307 SNEs.[23] This test was done as a 'trial' test before the proper running of codes, but it turned out to be useful results. This test helps us to roughly gauge the best fit value of H_0 using the SNE test. The results are summarized in **Table 7**, and **Figs. 17a-17e** show the resulting χ^2 contour plots (in the same scale for comparison purposes).

H_0 (km s^{-1} Mpc^{-1})	$\Omega_{m,0}$	n	χ^2_{min}
68	0.09	-0.86	321.95
69	0.34	0.10	314.55
70	0.42	1.34	310.75
71	0.44	2.74	310.79
72	0.45	5.14	314.85

Table 7: Best Fit Values of $\Omega_{m,0}$ and n for $f_1(T)$ at different H_0 using the SNE Test

The table showed that the $f_1(T)$ model favored the value of $H_0 = 70 \pm 1$km s^{-1} Mpc^{-1}, and a mass density of $0.42^{+0.02}_{-0.02}$. This high value compared to the results in **Chapter 5** is due to the different SNE data used. The contour plots showed that the higher the value of H_0, the higher the uncertainty for n. To improve this result, one could attempt to fit the model with the updated Union2.1 dataset.

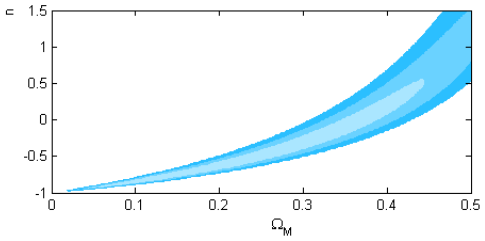

Fig. 17a: SNE Test for $f_1(T)$ at $H_0 = 68$km s^{-1} Mpc^{-1}

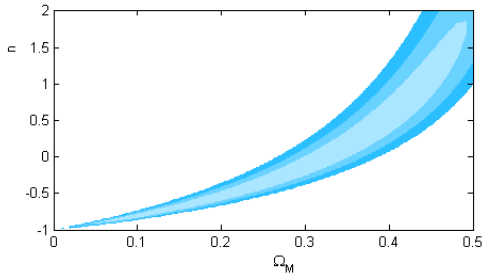

Fig. 17b: SNE Test for $f_1(T)$ at $H_0 = 69$km s^{-1} Mpc^{-1}

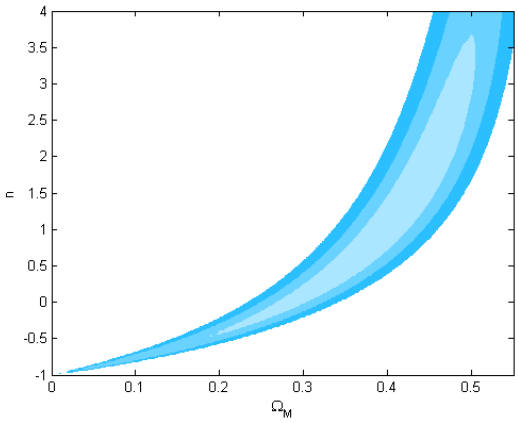

Fig. 17c: SNE Test for $f_1(T)$ at $H_0 = 70\text{km s}^{-1}\text{ Mpc}^{-1}$

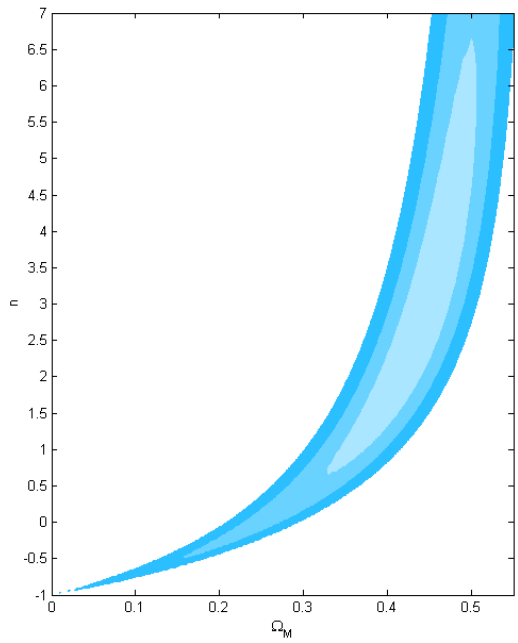

Fig. 17d: SNE Test for $f_1(T)$ at $H_0 = 71\text{km s}^{-1}\text{ Mpc}^{-1}$

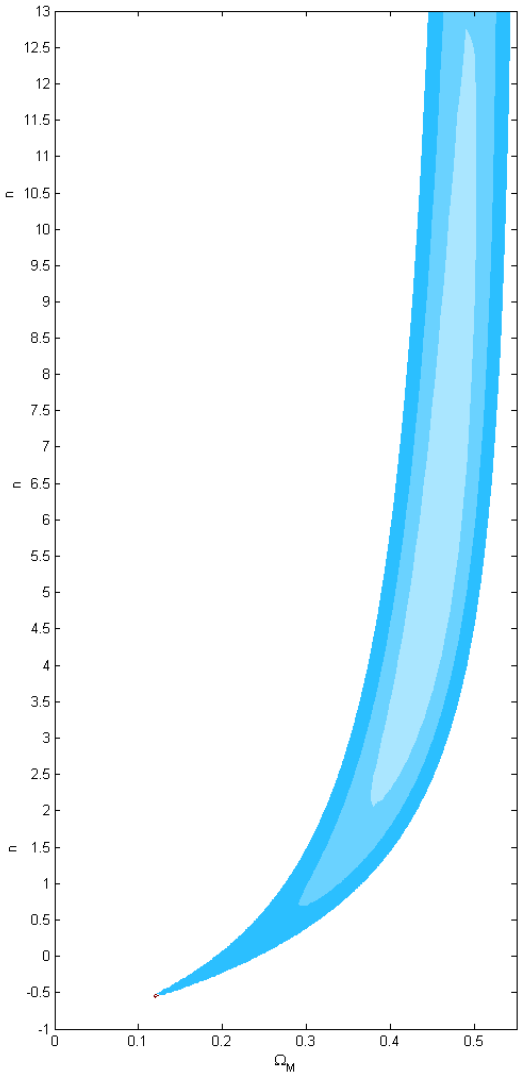

Fig. 17e: SNE Test for $f_1(T)$ at $H_0 = 72\text{km s}^{-1}\text{ Mpc}^{-1}$

B2 Analytical Marginalization v.s. Minimized χ^2 Method

As mentioned in **Chapter 4**, the analytical marginalization and minimized χ^2 method in the SNE test yield equivalent results, as their equations differ by 2 constant terms. The graphs below show the two different SNE tests on $f_1(T)$ using the Union1.0 data. The results in **Table 8** and the contour plots below both act as proof that both methods indeed yield similar results. Once again, the values of $\Omega_{m,0}$ are higher than those obtained in section 5, due to the fact that the older Union1.0 data was used. The Union1.0 data suggests a non-zero n value, and thus showed a deviation from the ΛCDM Model.

Method	$\Omega_{m,0}$	n	χ^2_{min}
Analytical Marginalization	0.43	1.91	319.71
Minimized χ^2	0.43	1.92	310.28

Table 8: Best Fit Values of $\Omega_{m,0}$ and n for $f_1(T)$ at different H_0 using the SNE Test

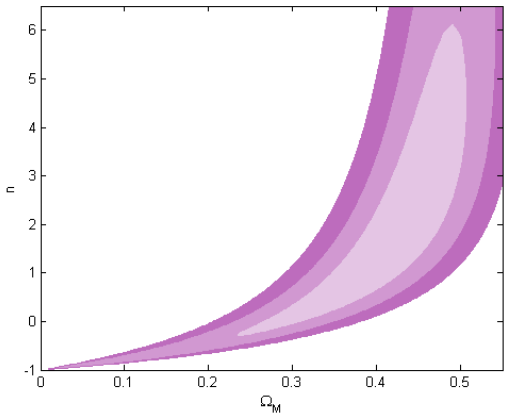

Fig. 18a: SNE Test on $f_1(T)$ using Analytical Marginalization

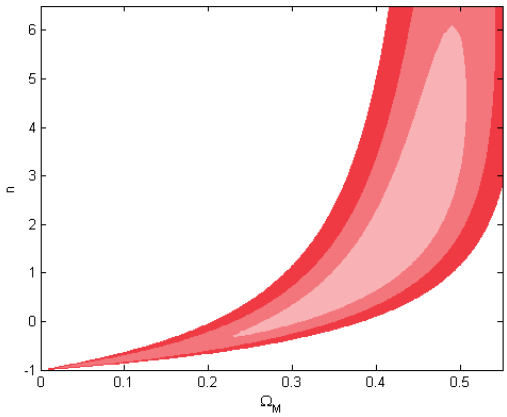

Fig. 18b: SNE Test on $f_1(T)$ using Minimized χ^2 Method

B3 GRB Test Results

As mentioned in **Chapter 3**, the GRB test is a very weak constraint, and does not significantly affect the results of combined χ^2 tests overall. The graphs in the following page show the contour plots of the GRB test. The test is conducted using data of 5 redshift values and the correlation matrix suggested by Xu.[49] It can be seen that the constraints are indeed very weak, and their best-fit parameters are very much different from those obtained from the SNE, CMB/BAO and OHD test. Thus, the GRB test is not a good observational constraint for cosmological models at the moment. The results obtained from the GRB tests are tabulated in **Table 9**.

Function	$\Omega_{m,0}$	n	χ^2_{min}
$f_1(T)$	0.02	-0.97	0.864
$f_2(T)$	0.85	-0.27	0.413
$f_3(T)$	0.13	-0.64	0.873

Table 9: Best Fit Values of $\Omega_{m,0}$ and n for the $f(T)$ models using the GRB Test

The common results obtained from the 3 functions, is that the models favor a negative n value. The values of $\Omega_{m,0}$ obtained are highly inconsistent, and they have a huge range between 0 and 0.9. Indeed, the GRB test is not as reliable as the rest, and cannot be used as a stand-alone observational constraint.

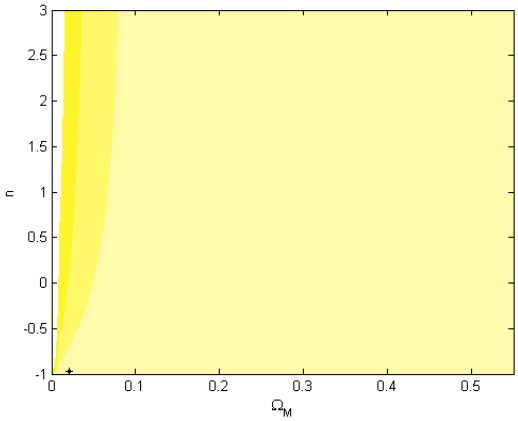

Fig. 19a: GRB Test for $f_1(T)$

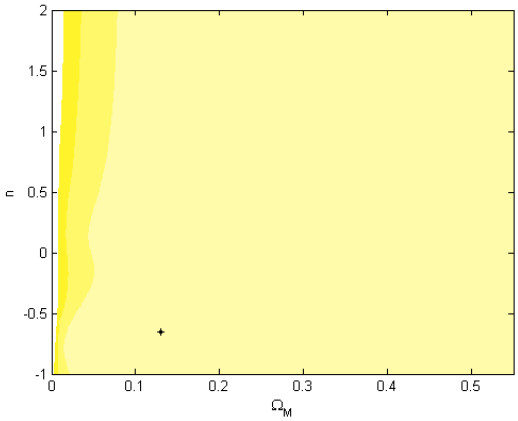

Fig. 19b: GRB Test for $f_3(T)$

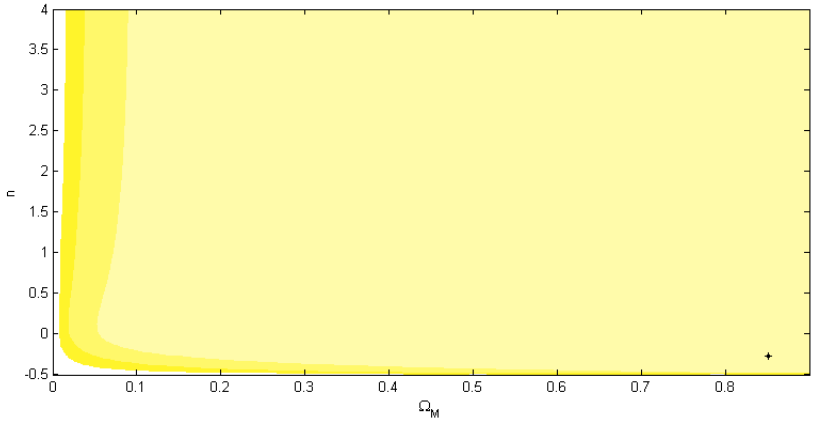

Fig. 19c: GRB Test for $f_2(T)$

APPENDIX C: $f(T)$ MODELS BY OTHERS

The following table summarizes a few $f(T)$ models proposed by various authors in the recent years, tabulated with their best fit values.

Year	Author	$f(T)$ Function	Best Fit Values	Remarks
2010	Bengochea[29]	$f(T) = T - \frac{\alpha}{(-T)^n}$	$\Omega_{m,0} = 0.29$ $\chi^2_{min}/\nu = 0.67$ (S2+B/C+G+O)*	Similar to $f_1(T)$ proposed in this work.
2010	Linder[38]	$f(T) = T - \alpha T\left(1 - e^{\frac{pT_0}{T}}\right)$	$\Omega_{m,0} = 0.272$ $\chi^2_{min}/\nu = 0.976$ (S2+B+C)	Linder merely formulated this function based on his $f(R)$ model in a previous work. Fitting conducted by Wu & Yu.[1]
2011	Bamba *et. al*[50]	$f(T) = \beta T_0\sqrt{\frac{T}{qT_0}}\ln\left(\frac{qT_0}{T}\right) - T\left(1 - e^{u\frac{T_0}{T}}\right)$	$\Omega_{m,0} = 0.282$ $\chi^2_{min} = 544.56$ (S2+B+C)	Model motivated to realize the crossing of the phantom divide line.
2011	Myrzakulov[51]	$f(T) = \alpha T + \beta T^{\delta}\ln T$	-	Myrzakulov merely constructed the solutions for his function.
2011	Wu & Yu[3]	$f(T) = \alpha(-T)^n \tanh\frac{T_0}{T}$	$\Omega_{m,0} = 0.282$ $\chi^2_{min} = 543.948$ (S2+B+C)	Motivated to realize the crossing of the phantom divide line.
		$f(T) = \alpha(-T)^n\left(1 - e^{\frac{pT_0}{T}}\right)$	$\Omega_{m,0} = 0.267$ $\chi^2_{min} = 544.213$ (S2+B+C)	

Table. 10: $f(T)$ Models in the Work of Others

* S2 = SNE 1a (Union 2.0 data), B = BAO, C = CMB, C/B = CMB/BAO Combined, G = GRB and O = OHD.

REFERENCES

1. P. Wu and H. Yu (2010) Physics Letters B **693** (4), 415-420.
2. I. Keisuke and Y.C. Ong (2013). Journal of Cosmology and Astroparticle Physics **2013** (06), 029.
3. P. Wu and H. Yu (2011). The European Physical Journal C **71** (2), 1-6.
4. Wikipedia, *Ultimate Fate of the Universe*. Retrieved 12/3/2014, from http://en.wikipedia.org/wiki/Fate_of_the_Universe.
5. S. C. C. Ng (2013). Lecture notes for *PC4232 Cosmology*, Department of Physics, National University of Singapore.
6. Wikipedia, *Ricci Curvature*. Retrieved 12/3/2014, from http://en.wikipedia.org/wiki/Ricci_curvature.
7. Wikipedia, *Scalar Curvature*. Retrieved 12/3/2014, from http://en.wikipedia.org/wiki/Ricci_scalar.
8. Wikipedia, *Action (Physics)*. Retrieved 12/3/2014, from http://en.wikipedia.org/wiki/Action_(physics).
9. Q. Wang (2013). Lecture notes for *PC4248 Relativity*. Department of Physics, National University of Singapore.
10. R. Aldrovandi and J. G. Pereira (2013). *Teleparallel Gravity: An Introduction*. Springer, London.
11. H. I. Arcos and J. G. Pereira (2004). International Journal of Modern Physics D **D13**, 2193-2240.
12. K. Hayashi and T. Shirafuji (1979). Physical Review D **19** (12), 3524-3553.
13. Wikipedia, *Connection (Mathematics)*. Retrieved 25/3/2014 from http://en.wikipedia.org/wiki/Connection_(mathematics).
14. G. R. Bengochea and R. Ferraro (2009), Physical Review D **79** (12), 124019.
15. J. V. Nalikar (2002). *An Introduction to Cosmology*. Cambridge University Press, United Kingdom.
16. M. Kowalski, D. Rubin, G. Aldering *et. al* (2008). The Astrophysical Journal **686** (2), 749.
17. S. Tsujikawa (2011). *Dark Matter and Dark Energy*, Vol. 370, pp. 331-402. Springer, Netherlands.
18. N. Deruelle, M. Sasaki, Y. Sendouda and A. Youssef (2012). Journal of High Energy Physics **2012** (9), 1-21.
19. Y. C. Ong, K. Izumi, J. M. Nester and P. Chen (2013). Physical Review D **88** (2), 024019.
20. Wikipedia, *Supernova*. Retrieved 26 March 2014, from http://en.wikipedia.org/wiki/Supernova.
21. Hubblesite, *The Progenitor of Type Ia Supernovae*. Retrieved 15/3/2014, from http://hubblesite.org/newscenter/archive/releases/star/supernova/2004/34/image/d/.
22. E. J. Copeland, M. Sami and S. Tsujikawa (2006). International Journal of Modern Physics D **15** (11), 1753-1935.
23. Supernova Cosmology Project. Retrieved 26/3/2014, from http://supernova.lbl.gov/.
24. W. Hu, N. Sugiyama and J. Silk (1997). Nature **386** (6620), 37-43.

25. Ø. Elgarøy and T. Multamäki (2007). Astronomy and Astrophysics Manuscripts **471** (1), 65-70.
26. Y. H. J. Soo (2013). *Observational Constraints on Dark Energy,* Report for Undergraduate Research Opportunities Programme in Science (UROPS). Department of Physics, National University of Singapore.
27. D. J. Eisenstein and W. Hu (1998). The Astrophysical Journal **496**, 605-614.
28. G. E. Addison, G. Hinshaw and M. Halpern (2013). arXiv:1304.6984 [astro-ph.CO].
29. G. R. Bengochea (2011). Physics Letters B **695** (5), 405-411.
30. R. Jimenez and A. Loeb (2001). The Astrophysical Journal **573**, 37-42.
31. D. Stern, R. Jimenez, L. Verde *et. al.* (2010). Journal of Cosmology and Astroparticle Physics **2010** (02), 008-008.
32. Wikipedia, *Gamma-ray burst*. Retrieved 27/3/2014, from http://en.wikipedia.org/wiki/Gamma-ray_burst.
33. NASA Mission Science, *Gamma Rays*. Retrieved 17/3/2014 from http://missionscience.nasa.gov/ems/12_gammarays.html.
34. J. Byun (2011). *Can Gamma-Ray Bursts Be Used As Standard Candles*. Department of Astronomy, Cornell University.
35. Y. Wang (2008). Physical Review D **78** (12), 123532.
36. W. Hao (2010). Journal of Cosmology and Astroparticle Physics **2010** (08), 020.
37. L. Samushia and B. Ratra (2010). The Astrophysical Journal **714** (2), 1347-1354.
38. E. V. Linder (2010). Physical Review D **81** (12).
39. W. H. Press, S. A. Tueukolsky, W. T. Vetterling and B. P. Flannery (1986). *Fortran Numerical Reciples, 2 ed*. Cambridge University Press, United Kingdom.
40. E. Komatsu, J. Dunkley, M. R. Nolta *et. al* (2009). The Astrophysical Journal Supplement Series **180** (2), 330.
41. A. G. Riess, L. Macri, S. Casertano *et. al* (2009). The Astrophysical Journal **699** (1), 539-563.
42. E. Gaztañaga, A. Cabré and L. Hui (2009). Monthly Notices of the Royal Astronomical Society **399** (3), 1663-1680.
43. H. S. P. Lim (2013). Lecture Notes for *PC3236 Computational Methods in Physics*, Department of Physics, National University of Singapore.
44. Wikipedia, *Gaussian Quadrature*. Retrieved 20/3/2014 from http://en.wikipedia.org/wiki/Gaussian_quadrature.
45. M.O. Farooq and R. Bharat (2013). The Astrophysical Journal Letters **766**(1): L7.
46. S. Capozziello, V. F. Cardone, H. Farajollahi and A. Ravanpak (2011). Physical Review D **84** (4), 043527.
47. V. F. Cardone, N. Radicella and S. Camera (2012). Physical Review D **85** (12).
48. S. Nesseris, S. Basilakos, E. N. Saridakis and L. Perivolaropoulos (2013). Physical Review D **88** (10).
49. L. Xu (2012). Journal of Cosmology and Astroparticle Physics **1204**, 025.
50. K. Bamba, C. Q. Geng, C. C. Lee and L. W. Luo (2011). Journal of Cosmology and Astroparticle Physics **2011** (01), 021-021.
51. R. Myrzakulov (2011). The European Physical Journal C **71** (9), 1-8.